**Marine and Petroleum Geology**
November 2020, Volume 121, Pages 104581 (26p.)
https://doi.org/10.1016/j.marpetgeo.2020.104581
https://archimer.ifremer.fr/doc/00641/75269/



# Seagrass-related carbonate ramp development at the front of a fan delta (Burdigalian, New Caledonia): Insights into mixed carbonate-siliciclastic environments

Tournadour Elsa [1, 2, *], Fournier F. [3], Etienne S. [1, 2], Collot Julien [2], Maurizot P. [2], Patriat Martin [4], Sevin B. [2], Morgans H.E.G. [5], Martin-Garin B. [3], Braga J.C. [6]

[1] Adecal Technopole, 1 bis Rue Berthelot, Doniambo, B.P. 2384-98 846, Nouméa, New Caledonia
[2] Service Géologique de Nouvelle-Calédonie, DIMENC, B.P. 465, 98845, Nouméa, New Caledonia
[3] Aix Marseille Univ, CNRS, IRD, INRAE, Coll France, CEREGE, Case 67, 3, 13331, Marseille Cedex 03, France
[4] IFREMER, Unité Géosciences Marines, 29280, Plouzané, France
[5] GNS Sciences, PO Box 30368, Lower Hutt, 5040, New Zealand
[6] Universidad de Granada, Departamento de Estratigrafía y Paleontología, Avenida de La Fuente Nueva, 18071, Granada, Spain

* Corresponding author : Elsa Tournadour, email address : elsa.tournadour@gouv.nc

**Abstract :**

Past shallow-water carbonate environments of the main island of New Caledonia (NC) have been subject to high terrigenous influx derived from the erosion of ultramafic obducted nappes and are therefore a relevant case study for characterizing neritic carbonate production in mixed carbonate-siliciclastic systems under a tropical climate. More particularly, we focused on Burdigalian carbonate sedimentary records cropping out on the western coast of NC, in the Népoui area. Based on a comprehensive sedimentological study of cores and outcrops, we established a new depositional model of an alluvial fan to carbonate ramp transition. Shallow-water (euphotic) carbonate production was dominated by seagrass-related biota and corals derived from small-sized bioconstructions. Extensional tectonics and associated normal faulting, driven by post-obduction isostatic rebound, favored carbonate ramp aggradation and preservation. The carbonate ramp was incised by conglomerate-filled terminal distributary channels, which indicate that terrigenous inputs remained significant during marine transgression and did not inhibit the development of seagrass and scleractinian carbonate factories. Phytal substrates induced by seagrass and/or macro-algae seafloor colonization strongly controlled the nature of carbonate production and promoted the accumulation of foraminiferal-coralline algal sediments. Seagrass development at the front of the fan delta is interpreted to have controlled the preservation of a diverse and significant carbonate production by reducing water turbidity and by limiting the risk of suffocation for filter-feeding biota in such a high terrigenous influx setting.

**Highlights**

► Extensive development of seagrass carbonates occurs at the front of tropical fan delta. ► Seagrass meadows development favored carbonate production and preservation. ► The long-term preservation of the depositional system is due to the post-obduction subsidence regime.

**Keywords** : Miocene, seagrass, tropical carbonates, terrigenous inputs, alluvial fan, facies association, New Caledonia

# 1. INTRODUCTION

Mixed carbonate-siliciclastic depositional systems are characterized by a high vertical and lateral variability in facies and lithologies, which results from the interplay between carbonate production and terrigenous supply. Such complexity makes difficult the sequence stratigraphic interpretation of mixed systems (Zeller et al., 2015) and complicates the prediction of reservoir architectures from subsurface data (McNeill et al., 2004).

Mixed systems have been commonly subdivided into temporal phases of either dominant carbonate or siliciclastic deposition by applying the concepts of reciprocal sedimentation (Wilson, 1967). According to this model, siliciclastic deposits prevail during low sea level periods whereas carbonate facies dominate during transgressions and highstands. However, this model, often used in ancient case studies (e.g. Permian Capitan margin: Silver & Todd, 1969; Kerans & Tinker, 1999) has been shown to be inadequate for describing several quaternary (e.g. Great Barrier Reef: Page et al., 2003; Harper et al., 2015; New Caledonia: Le Roy et al., 2019) and ancient mixed carbonate-siliciclastic systems (e.g. Late Jurassic northeastern France: Olivier et al., 2004; Jurassic-Cretaceous Neuquén basin, Argentina: Zeller et al., 2015). The deviations from

the reciprocal sedimentation model may be related to increased siliciclastic inputs during transgression as a result of regional climate changes, reworking and dispersing of previously deposited terrigenous sediments (Harper et al., 2015) or steeper fluvial profile compared to shoreline trajectory (Catuneanu, 2019). In addition, continued high carbonate production during sea level lowstands and/or periods of high terrigenous inputs go against the applicability of reciprocal sedimentation concepts (Zeller et al., 2015). Carbonate production and the nature of carbonate producers are therefore a key parameter to be considered for the prediction of depositional models and stratigraphic architectures in mixed systems. Moreover such predictions are complicated by the interplay between carbonate production and siliciclastic inputs. Terrigenous influx is known to be a significant factor controlling carbonate production since it leads to increased water turbidity, thus reducing available light for light-dependent organisms and to suffocation of filter-feeding biota due to high sedimentation regimes (e.g. Rogers 1990; Fabricius 2005). Many studies have shown that prolonged exposure to terrigenous discharge from rivers has a negative impact on shallow-water carbonate production, particularly in coral reefs (Rogers 1990; Van Katwijk et al. 1993; Fabricius 2005). In contrast, such a negative impact of terrigenous inputs on neritic carbonate production has been contradicted in different Quaternary and ancient tropical carbonate systems from the Indo-Pacific (e.g. Wilson, 2005; Perry et al., 2012; Novak and Renema, 2015; Santodomingo et al., 2015) and Mediterranean domains (e.g. Corsica: Tomassetti et al., 2013; Sardinia: Vigorito et al., 2012; Ligurian Alps: Brandano et al., 2015; Turkey: Bassant et al., 2005), and many examples of barrier-reef systems developing on terrigenous shelves were documented in modern environments (The Great Barrier Reef in Australia: e.g. Belperio, 1983; Orpin et al., 2004; Puerto-Rico: Ryan-Mishkin et al., 2009; Belize shelf: Mc Neill et al., 2010; Gulf of Mexico: Hernandez-Arana et al., 2015). These numerous examples have demonstrated the great capacity of photozoan, coralgal production to adapt to strong terrigenous inputs. However, even though seagrass-related biota has been reported in various mixed carbonate-siliciclastic systems (e.g. Reuter et al., 2011; Sola et al., 2013; Beavington-Penney et al., 2004), relatively low attention has been paid on the resilience of

seagrass carbonate factories to strong terrigenous discharges (Mateu-Vicens et al., 2012). Additionnaly, although Cenozoic seagrass deposits are well known from the Caribbean (Eva, 1980), the Mediterranean (e.g. Mateu-Vicens et al., 2008; Brandano et al., 2009; Bassi and Nebelsick, 2010; Sola et al., 2013; Tomassetti et al., 2016) to the Indo-Pacific (e.g. Chaproniere, 1975; Beavington-Penney et al., 2004; Reuter et al., 2011; Haig et al., 2020) areas, complete depositional models of seagrass-influenced carbonate systems subject to high terrigenous supplies are lacking.

The Upper Népoui Formation (Burdigalian), cropping out on the western margin of New Caledonia (South-West Pacific), is a mixed shallow-marine depositional system where continuous terrigenous inputs derived from post-obduction erosion of ultramafic nappes were supplied into shallow-water ramp environments where a significant seagrass-related, and scleractinian carbonate production occurred (Maurizot et al., 2016). Such spatially well-constrained outcrops thus represent a relevant case study for understanding the ecological and physical processes that control the architecture and evolution of tropical, seagrass-dominated carbonate systems which are subject to high terrigenous supplies.

A comprehensive sedimentological study of the Burdigalian mixed system has been performed, based on newly acquired core data as well as new outcrop descriptions. On the basis of the detailed geological mapping and logging of sedimentary units, coupled with micro- and macro-scale petrographic and sedimentological characterisation of the carbonate and terrigenous deposits, the present work aims at: 1) constructing an original depositional model of the transition from an alluvial-fan to a seagrass-dominated carbonate ramp, 2) assessing the role of potential controlling factors such as relative sea level fluctuations, nutrient supplies and water turbidity on the depositional architecture of mixed carbonate-siliciclastic systems, and 3) discussing the significance of seagrass-related carbonate factories in tropical environments subject to high-terrigenous influx.

The resulting depositional architecture constitutes a valid and original model for potential hydrocarbon reservoirs in mixed carbonate-siliciclastic ramps forming in tropical setting.

# 2. GEOLOGICAL SETTING

## 2.1 Geodynamic framework of the New Caledonian western margin

The New Caledonian main island, Grande Terre, is located in the South West Pacific (Fig.1), at the north-eastern tip of Zealandia, a large and mostly submerged piece of thinned continental crust inherited from the cretaceous break-up of eastern Gondwana (Mortimer et al., 2017). Indeed, from Late Cretaceous to Paleocene, a rifting phase followed by seafloor spreading in Tasman Sea led to the isolation of Zealandia (Gaina et al., 1998). During the Eocene, New Caledonia underwent a convergence phase that led to the NE–SW emplacement of various nappes, including the prominent mantellic Peridotite Nappe (Paris, 1981; Cluzel et al., 1994; Aitchison et al., 1995; Cluzel et al., 2001; Cluzel et al., 2012). During obduction, the New Caledonia Basin, which is located west of Grande Terre, reacted as an asymmetrical flexural basin, and is now filled by 6 km-thick post-obduction sediments (Collot et al., 2008).

The tectonic and sedimentary evolution of Grande Terre during the post-obduction period (Oligocene-present) remains debated. Most authors agree that this period is characterized by an uplift of Grande Terre driven by post-obduction isostatic rebound (Moretti & Turcotte 1985, Lagabrielle & Chauvet, 2008, Collot et al., 2017). This uplift is interpreted as being at the origin of the collapse of both the western and eastern margins through large scale normal faults together with the development of a deepwater fold and thrust belt at the foot of the western margin of New Caledonia (Lagabrielle & Chauvet, 2008, Collot et al., 2017). However, based on the subduction-related geochemical signatures of the Koum and St Louis granitoids intruding the Peridotite Nappe, Cluzel et al. (2005) and Paquette and Cluzel (2007) suggested that a short-

lived east-dipping Oligocene subduction of the New Caledonia Basin occurred beneath Grande Terre.

More recently, since the Plio-Quaternary, Grande Terre has been also affected by antithetic vertical motions between its western and southeastern margins. Indeed, based on drillings performed both on fringing reefs and on the barrier reef, Cabioch et al. (1999) suggested that a subsidence of the western margin of New Caledonia allowed the aggradation of the barrier reef and the associated lagoon. Montaggioni et al. (2011) estimated this subsidence to be higher than 0.08 mm · $yr^{-1}$ since 1 Ma ago. Conversely, along the southeastern margin of New Caledonia, a ca. 10 m uplift of reefs is observed in the area of Yaté and Pines Island (Cabioch et al., 1996). These reef uplifting is thought to be the result of the flexure of the lithospheric plate entering into the New Hebrides subduction (Dubois et al., 1974; Lafoy et al., 1995).

## 2.2 Geological setting of the Népoui area

The mixed siliciclastic carbonate deposits of the Népoui Group crop out along the western margin of New Caledonia, in front of the peridotite massifs of Kopéto and Boulinda. They unconformably rest on both the Népoui Eocene Flysch and the Poya Terrane (Figs.2A and B). The Népoui Flysch, dated from the late Eocene by micropaleontologic analyses, is considered as a syn-obduction formation based on its mafic lithological composition and its deformed state (Cluzel et al., 1998). It constitutes the youngest formation located beneath the allochtonous Peridotite Nappe, which would constrains the oldest possible age of the end of obduction at 34 Ma. The Poya Terrane comprises mid ocean ridge basalts and abyssal sediments, dated from the Late Cretaceous to the latest Paleocene based on radiolarian fauna, and is situated at the base of the Peridotite Nappe (Paris, 1981; Cluzel et al., 1997) (Figs.2A and 2B).

First descriptions of the Népoui Group considered a relatively simple vertical succession involving a lower fluvio-deltaic unit, named the Pindaï Conglomerates, overlain by shallow

164 marine limestones, initially attributed to the Early to Middle Miocene (Gubler & Pomeyrol,
165 1948 ; Coudray, 1975 ; Paris, 1981) (Figs.2A and B). More recently, Maurizot et al. (2016)
166 discovered a new limestone unit below the Pindaï Conglomerates, on the Chapeau Chinois
167 outcrops and in the 103 m deep S4 well (see location on Fig. 2), which reached the unconformity
168 separating post-obduction miocene deposits from the syn-obduction eocene Népoui Flysch
169 (Fig.2B and Fig.3). These authors consequently subdivided the mixed system of Népoui into
170 three formations and restricted the lower limestone formation to the Aquitanian and the upper
171 limestone formation to the Burdigalian based on six strontium isotope measurements perfomed
172 on preserved Mg-calcite from echinoid spines, combined with benthic and planktonic
173 foraminiferal biostratigraphy (Fig. 3). The lower formation (Lower Népoui Formation) is a
174 dominantly carbonate interval composed of three members, from base to top: the A1 Chapeau
175 Chinois Member, the A2 Operculina Green Sands Member and the A3 Xuudhen Limestone
176 Member (Fig. 3). Above, the strictly siliciclastic, fluvio-deltaic Pindaï Conglomerate Formation, is
177 assigned to the Burdigalian, yet no direct biostratigraphic or radiometric datings were
178 performed on that interval. The upper formation (Upper Népoui Formation) is made of mixed
179 carbonate-siliciclastic, shallow water deposits, Burdigalian in age, which are subdivided into two
180 members: the Wharf Member and the Népü Limestone Member (Fig. 3). In this paper, we argue
181 that the Pindaï Conglomerates are part of the Upper Népoui Formation, similarly to the
182 lithostratigraphic framework proposed by Sevin et al. (2014). Following this scheme, the Upper
183 Népoui Formation comprises the B1 Pindaï Conglomerate Member, the B2 Wharf Member and
184 the B3 Népü Limestone Member (Fig. 3). A dominant seagrass-related carbonate production
185 prevailed in the euphotic area of the Aquitanian and Burdigalian ramps (Maurizot et al., 2016),
186 even though scattered scleractinian colonies are common in both systems.
187
188 Finally, the post-Burdigalian Muéo Formation unconformably rests on the Népoui Upper
189 Formation on the Pindaï and Muéo peninsulas (Fig.2A). It primarily comprises extensive lateritic
190 red muds with large silicified blocks and reworked lateritic ferricretes (Paris, 1981). In former

191 studies, this formation was correlated with the Pindaï conglomerates, which led to some degree
192 of confusion (Paris, 1981).
193
194 In the offshore domain, seismic profiles revealed a 200 km along-margin and 50 km into the
195 basin deepwater fold and thrust belt in front of the Népoui area, interpreted as being gravity
196 driven (Rigolot & Pelletier, 1988; Collot et al., 2017) (Fig.1). Faults associated with this failure
197 are deeply rooted in the New Caledonia Basin (ca. 5 km depth) and are interpreted as being in
198 continuity with major detachments onshore that is in agreement with the extensional tectonic
199 model suggested by Lagabrielle & Chauvet (2008).

## 3. DATA AND METHODS

Outcrops of the Népoui Group are restricted to an area of about 100 $km^2$ that includes the Pindaï, Muéo, Nékoro, and Béco peninsulas, as well as the islands and islets of Grimault, Didot and Longue (Fig.4). This study focused on the Burdigalian Upper Nepoui Formation (Fig.3). The overall stratigraphic succession is 80 m–thick and is slightly tilted (< 10°) towards the SSW, i.e. towards the present day lagoon and Quaternary barrier reef (Fig.2). The most recent study dedicated to the Népoui Group was based on the description of a 103 m deep cored well, S4, in combination with its stratigraphic continuity exposed on the outcrops of the Chapeau Chinois and Wharf areas (Maurizot et al., 2016) (Fig. 4). In order to improve the architectural characterization of the Upper Népoui Formation (Burdigalian), the existing dataset was complemented by a new, 170 m-long cored well, S2 (Fig. 4). The latter is located only a few kilometers away from the main outcrops of the Pindaï peninsula and reveals the spatial variability system in a proximal to distal direction, following a NNE–SSW transect. Additionally, we included nine shallower drilled boreholes (20 to 30 m long) and detailed sedimentological descriptions of coastline outcrops of the Pindaï and Beco peninsula and of the Grimault, Didot and Longue islets, in order to constrain the depositional models and the stratigraphic architectures (Fig. 4). Based on this new dataset, we performed a detailed sedimentological analysis at the 1:50 scale using a classical “facies association” approach (eg. Allen, 1983; Miall, 1985; Posamentier & Walker, 2006). The outcrops and S2 core data were investigated by logging 7 key sections, which were summarized in 1:500 scale synthetic logs presented in Fig. 18. Depositional facies were defined based on sedimentary structures, depositional textures and biological composition identified from outcrops, cores and thin-sections. A total of 100 thin-sections from the Upper Népoui formation were used for microfacies characterization (texture, skeletal composition, diagenetic features). Additionally, 22 thin-sections were point-counted by using the JMicroVision software on the basis of 300 points to quantify the bioclastic composition of the sand-grained skeletal fraction of carbonates. Facies were grouped into facies associations, which were interpreted in terms of depositional environments. Finally, the lateral and vertical

227 stratigraphic distribution of facies associations allowed a well-constrained depositional model to
228 be proposed.

# 4. RESULTS

## 4.1 Facies association analysis

The Upper Népoui Formation is a lithologically heterogeneous and sedimentologically complex succession. The spatial and vertical distribution of the sedimentary facies, together with their stacking patterns further permits to gather them into eight facies associations that are thought to reflect distinctive depositional environments (Fig. 5). We identify continental deposits (FA1, FA2 and FA3) within the B1 Member of the Pindaï Conglomerates, shallow-marine sandstone deposits (FA4 and FA5) for the B2 Wharf Member and shallow-water carbonate deposits (FA6, FA7, FA8) typifying the B3 Népü Limestone Member. These facies associations are detailed in the following sections.

### *FA1- Proximal alluvial fan (Fig. 6)*

*Description:* in the northeastern part of the Pindaï Peninsula and on the Muéo Peninsula along the "*piste de roulage"* outcrops (see location Fig. 4), the Pindaï Conglomerates display well-rounded, moderately- to poorly-sorted pebbles in a coarse- to fine-grained sandy matrix (Fig. 6A). These polygenic conglomerates are composed of mafic and ultramafic clasts (serpentinites, serpentinised peridotites, dolerites, gabbros) as well as ferricrete clasts. They can reach 1 m in diameter but their average size is 30-40 cm (Fig. 6A, B and C). In the western part of the Muéo Peninsula, these conglomerates rest unconformably on the Népoui Eocene Flysch (Fig. 6E and 6F). Two fining upward conglomeratic to sandy successions are here exposed. They comprise matrix-supported, disorganized to normally graded conglomerates with erosive base, that evolve vertically towards gravelly sandstones with faint trough cross-bedding highlighted by gravels and pebbles (Fig. 6D and 6F). Although pebble orientation is in most places chaotic, a preferential north-dipping clast imbrication is observed, suggesting a north to south dominant transport. This orientation is confirmed by the presence of N20° oriented groove marks at the base of the second fining upward succession.

255

256 *Interpretation:* within the conglomeratic facies, the matrix-supported fabric, poor sorting of
257 clasts combined with the apparent lack of tractive sedimentary structures are consistent with
258 subaerial debris flow processes (Blair & McPherson 1994; Blair 1999). In turn, more structured
259 conglomerates and overlying cross-bedded gravelly sandstones are consistent with bedload
260 transport and tractive deposition by high density flows, and would possibly correspond to
261 braided-river barforms (Bluck, 1979; Miall, 1985). We therefore interpret this facies association
262 as recording deposition within the proximal part of an alluvial fan, where surficial braided
263 distributary channels can develop on top of alluvial fan debris flow lobes (e.g. sheetflood
264 dominated alluvial-fan model of Blair & McPherson, 1994). The lack of preserved floodplain
265 deposits is an additional evidence to favor an alluvial fan setting over a fluvial channel belt. In
266 addition, the lack of angular clasts in these facies is of note. Here, the subrounded to rounded
267 character of boulders and pebbles does not appear to be directly linked with flow transport
268 distance. Indeed, weathering of peridotites under a humid tropical climate can promote the *in*
269 *situ* formation of rounded blocks in saprolite layers (Trescases, 1975) (Fig. 6B). However, in the
270 absence of valuable geometrical constraints due to outcrop discontinuity, an alternative
271 interpretation where structureless conglomerates represent the basal part of channel-fills rather
272 than unconfined debris-flow lobes cannot be entirely ruled out.

273

274 ***FA2- Distal alluvial fan*** (Fig. 7)

275 *Description:* in the East of the Pindaï Peninsula, the basal part of the Wharf outcrops (see
276 location Fig. 4) exhibits a fining and thinning upward succession whose base consists in pebble-
277 cobble (2 to 15 cm in diameter) oblique bedded conglomerates, in places with pebbles preserved
278 as residual vugs ("ghost pebbles"), within a coarse-grained sandstone matrix with floating
279 granules (Fig. 7A and 7B). Several decimeter-thick intervals of normally graded, coarse-grained
280 trough cross-bedded sandstones with granules overlie these conglomerates. The whole
281 succession is organized as meter-scale oblique bedsets with dips of around 15–20° toward the

SSW (Fig. 7B). The succession is topped by red to greenish-red medium to fine-grained trough cross-bedded sandstones (Fig. 7C) capped by a traceable surface highlighted by numerous roots and iron oxide concretions (Fig. 7A and 7D).

*Interpretation:* similarly to FA1, oblique bedded conglomerates can be interpreted as sand-gravel bars formed by the sediment discharge of a unidirectional high capacity flow (Allen, 1983; Miall, 1985). Trough cross-bedded sandstones are consistent with fluvial settings and are typically assigned to three dimensional dunes (Allen, 1963; Allen, 1983) which may be interpreted to develop as frontal splays of alluvial fans. In our case, the SSW orientation of bedsets, parallel to the known general transport direction, together with the grading of sandstones points to a downstream accretion of deposits at the mouth of a stream channel alluvial fan rather than lateral accretion within a river channel belt. At the top of the succession, the decrease in grain size, increase in plant debris, root traces and iron concretions can be interpreted as a planar abandonment surface and are consistent with paleosol development. This facies association is therefore interpreted as a recording deposition within the distal part of alluvial fans.

### *FA3- Fluvial channel-fills (Fig. 8)*

*Description:* at the north easternmost extremity of the Didot Islet (see location Fig.4), an isolated, erosive based, 5 m-thick conglomerate succession is exposed (Fig. 8A and 8B: channel 1). It comprises polygenic, mafic and ultramafic, 5 to 6 cm in diameter pebbles within a coarse- to very coarse-grained sandy matrix organized in graded beds with erosional trough-shaped bases, and meter-scale oblique sets, with a dominant SSE orientation (Fig. 8C). These deposits contain numerous and large silicified wood fragments (Fig. 8D) including trunks, up to 1 m long. Laterally, only a few tens of meters westwards, a similar 10 m-thick succession occurs (channel 2: Fig.8A). Both successions are overlain by an alternation of marly deposits and centimeter-

thick, fine- to very fine-grained calcareous sandstones with undifferentiated bioclasts and foraminifers (Fig. 8A).

*Interpretation:* these well-structured conglomerates are interpreted as resulting from bedload transport, most likely within a coarse braided river system (Allen, 1963; Miall, 1977). Indeed, within such isolated channel-fills, individual trough cross-bedded sandstones record distinct phases of the channel fill. These small scale channel fills are interpreted to be deposits in fluvial to near-shore environments possibly as the downstream evolution of alluvial fan environments (FA1 and FA2).

### *FA4- Tidal sands (Fig. 9)*

*Description*: in the south of Longue Island (see location Fig.4), a 30 m-thick succession of very coarse to medium-grained cross-bedded sandstones, typically organized into sigmoidal megaripples, is exposed (Fig. 9A and 9D). These decimeter-thick sigmoidal bedsets extend over 2 to 5 m and show a 15° to 30° inclination of individual sets. Measurements of oblique set apparent dips reveal a main SE oriented progradation with subordinate orientations toward the W, NE, and E (Fig.18). Sigmoidal lamina sets can be locally erosional and commonly show cyclic increases and decreases in thickness within the same bed. Mud drapes, mud clasts, opposite ripples and bioturbation are present even though relatively scarce, possibly due an overall low fraction of mud-sized sediments. However, opposite megaripples (i.e. herring-bones) occur (Fig. 9B). In places, small-scale trough-cross ripple laminations are observed between bedsets. Frequent gravel lags and centimeter to decameter scale isolated lenses of well-rounded ultramafic pebbles within a calcareous muddy matrix are observed (Fig. 9C). These sandstones are primarily made of altered serpentinite grains and ferricrete fragments. Grains are coated with a fringing marine cement and separated from each other by drusy calcite cements (Fig. 9E).

*Interpretation:* The common preservation of alternating thicker and thinner sigmoidal foresets, erosional (reactivation) bounding surfaces, together with herring-bone cross-bedding, strongly suggests a tidal influence (spring-neap tide bundling). In addition, the apparent lack of storm and wave-related sedimentary features (ie. HCS, SCS, oscillating ripple laminations) point to the fact that the depositional environment is not significantly influenced by oscillating currents. The weak preservation of mud drapes and the lack of bioturbation could be seen as evidencing rapid bedform deposition by sustained, high-energy currents that reworked evidence for depositional pauses (eg. Willis et al., 1999). Consequently, cross-bedded sandstones are therefore thought to correspond to tidally influenced shallow marine sandstones, possibly conforming to tidal sand bars in an estuarine environment (Belderson et al., 1982; Reynaud & Dalrymple, 2012; Snedden & Dalrymple, 1999; Snedden, et al., 1999), or, alternatively, to distributary mouth bars in a tide-influenced delta front.

### *FA5- Subtidal sands (Fig. 10)*

*Description :* in the west of the Pindaï Peninsula, at the nautical base outcrops, as well as on the Didot Islet and the Beco Peninsula (see location Fig.4), fine to very fine-grained, tabular cross-bedded, typically bioturbated sandstones are exposed (Fig. 10A and 10D). The direction of apparent progradation is dominantly towards the SSW, yet a few measurements were found to be towards the E and NE (Fig. 14). Where grain size is finer, cross bedding is replaced by parallel laminations and isolated unidirectional ripples (Fig. 10B). Bioturbation is also more pronounced and trace fossils are more identifiable. Burrows include *Thalassinoides* and *Dactyloidites* (Fig. 10C). Additionally, numerous mafic and ultramafic granules are present, typically as lags or within burrow infills. In S2 well, cross-bedded and bioturbated sandstones exhibit a scarce and poorly diversified foraminiferal association dominated by poorly preserved *Miogypsina* and *Sorites*.

*Interpretation:* these sandstone facies are interpreted as sandy subtidal deposits downslope of FA-4 tidal sands. Their finer grain size, the ichnofacies (*Thalassinoides-Dactyloidite*s) and the lack of evidence for clear tidal features is consistent with deposition below the low tide limit. In addition, while *Thalassinoides* burrows may characterize diverse depositional settings from shallow to deep water environments (Bromley, 1996), *Dactyloidites* is usually considered to be restricted to sandy substrate in very shallow, shoreface environments (Uchman & Perversler, 2007). Finally, the scarcity and poor preservation of benthic foraminifers suggest these are not *in situ* but likely derived from neighboring euphotic to upper mesophotic environments (e.g. Hallock & Glenn, 1986; Pomar et al., 2014).

### *FA6- Subtidal, seagrass-related, low-angle carbonate ramp (Fig. 11)*

*Description:* outcrops from the B3 Népü Limestone Member are dominated by massive and chalky carbonates, which are commonly interbedded with centimeter to meter-thick intervals of ultramafic cobbles and boulders (Fig. 11D). Three dominant carbonate depositional facies have been identified within the FA-6 facies association: 1) FA6-1: Foraminiferal-coralline algal packstone-grainstones (Facies FB2 in Maurizot et al., 2016), 2) FA6-2: Scleractinian floatstone with a foraminiferal-coralline algal packstone-grainstone matrix (Facies FB1 in Maurizot et al., 2016), and 3) FA6-3: Scleractinian boundstones.

Foraminiferal-coralline algal packstone-grainstones (FA6-1) are organized into decimeter to meter-thick beds (Fig. 11B). They are dominated by benthic foraminifera and coralline algae, and include small proportions of mollusks and echinoderm fragments. Scleractinians may be present as sparse gravel to cobble-sized coral fragments but do not contribute significantly to the sand-sized skeletal fraction. It is likely that part of the sandy fraction deriving from corals is present as dissolved grains and has therefore been counted as indeterminate elements (<7 %). Vertical calcitic tubes of shipworm (teredinid) bivalves, 1 to 2 cm in diameter and 10 to 30 cm in length, may be common in a few beds (Fig. 11C). Packstones and grainstones exhibit very similar biological composition (Tables 1 and 2, Fig. 12) with high proportions of benthic foraminifers

(52 % and 46 % respectively), articulated coralline algae (13 % and 16 %) and encrusting coralline algae (17 % and 25 %). In both textures, the foraminiferal assemblage is dominated by benthic foraminifers which are known as common epiphytes (e.g. Chaproniere, 1975; Hallock et al., 2006; Pomar et al., 2014; Reich et al., 2014) such as the miliolid *Austrotrillina*, soritids (Fig. 13A, B, C, F), peneroplids, and calcarinids (*Neorotalia*) (Fig. 13D), which represent, in average, 30 % (packstones) and 27 % (grainstones) of the sand-sized bioclastic grains. Victoriellid encrusting foraminifers (Fig. 13E) are common (7 % in average but may reach up to 47 % of the sand-grained bioclastic fraction). They are always found isolated thus suggesting an unpreserved substrate of possible phytal origin. The alveolinid *Flosculinella* (Fig. 13C) is present in a few samples. *Gypsina* (Fig. 13E) is of common occurrence as well as other robust hyaline foraminifers such as amphisteginids and miogypsinids. Based on the nature of epiphytic (*Austrotrillina*, soritids, peneroplids and calcarinids) and potentially epiphytic (victoriellids) taxa which largely dominate the foraminiferal assemblage, three foraminiferal associations have been defined (Figs.12 and 14): 1) a porcelaneous-dominated epiphytic foraminiferal association dominated by *Austrotrillina*, soritids and peneroplids (77 % in average of the epiphytic foraminiferal composition, 45 % of the whole foraminiferal content) (Fig. 13A, B, C, F), 2) a rotalid-dominated epiphytic foraminiferal association dominated by *Neorotalia* (88 % in average of the epiphytic foraminiferal composition, 57 % of the whole foraminiferal content) (Fig. 13D) and 3) a victoriellid-dominated association (60 % of the whole foraminiferal content) (Fig. 13E). The coralline algal assemblage is composed of *Lithophyllum* gr. *pustulatum*, "*Lithophyllum pseudoamphiroa"*, *Corallina* and *Jania*. The green algae *Halimeda* is rare and has been observed in a very few samples (Fig. 13B). Sand-grained to gravel-grained lithoclasts (altered peridotites) mixed within the carbonate fraction are of common occurrence (Fig. 13B).

Scleractinian floatstones (FA6-2) are commonly interbedded within foraminiferal-coralline algal packstone-grainstones and conglomerate thin (0.10–1.0 meter-thick) beds (Fig. 11D). The foraminiferal assemblage is similar to that of the foraminiferal-coralline algal packstone-grainstones (Table 1) since it is dominated by benthic foraminifers with a large proportion of

epiphytes and coralline algae including both articulated and encrusting forms. The benthic foraminiferal association is composed of soritids, alveolinids (*Flosculinella*), miliolids (*Austrotrillina*), calcarinids (*Neorotalia*) together with significant proportions of victoriellids. amphisteginids, calcarinids and miogypsinids (*Miogypsina* and *Miogypsinoides*) are present in minor proportions. The scleractinian assemblage includes *Heliastrea, Stylophora, Goniopora, Porites, Siderastrea* and *Dipastraea* (Maurizot et al., 2016). Corals are mainly found as rubbles but rare *in-situ*, small-sized (< 50 cm thick, < 1m in diameter) coral bioconstructions (= scleractinian boundstone: FA6-3) have been observed interbedded within coral floatstone intervals (Fig. 11G).

A few kilometers away from the Wharf outcrops, at the S2 well, the B3 Member is significantly thicker (80 m), strongly dolomitized (Fig 11E), and displays karst features filled by reddish clay-rich sediments (Fig 11F).

<u>*Interpretation:*</u> in both foraminiferal-coralline algal packstone-grainstones and coral floatstones, the foraminiferal assemblage is dominated by taxa which are known as common epiphytes (flat, disk-shaped soritids, *Austrotrillina, Neorotalia*) and which suggests very shallow, euphotic environments with extensive development of seagrass meadows (e.g. Chaproniere, 1975; Pomar et al., 2014). Robust and rounded specimens of amphisteginids are also indicative of very shallow-water settings (Hallock & Glenn, 1986) and their diameter-thickness ratios (<2) suggest water-depth lower than 10 meters (Renema, 2005; Mateu-Vicens et al., 2009). Even though calcarinids such as *Neorotalia* may live on sandy substrates, they have been shown to prefer phytal substrate such as macro-algae (Renema, 2010; Reich et al., 2015), short filamentous algae (Renema, 2003) and seagrasses (Lobegeier, 2002). *Neorotalia* has been shown to be abundant in Oligo-Miocene seagrass facies (Fournier et al., 2004; Pomar et al., 2014). The *Flosculinella-Austrotrillina*-soritid association has been reported in various Neogene seagrass meadows environments (Chaproniere, 1975; Fournier et al., 2004; Hallock et al., 2006; Reich et al., 2014). Additionally, the general absence of preserved substrate suggests that victoriellids encrusted

non-calcified biota such as, possibly, seagrass leaves or rhizomes. The relatively high-mud content (packstone texture: Fig. 13A, B, C, D, E) also supports the interpretation of sea-grass environments (e.g. Brandano et al., 2009; Reuter et al., 2012; Mateu-Vicens et al., 2012). Additionally, abundance of articulated coralline algae is a common feature of seagrass meadow environments (e.g. Lukasik et al., 2000; James & Bone, 2007) even though they may be common in a wide range of shallow marine environments. Similar bioclastic composition present in grainstones which may reflect a deposition in high-energy, non- or poorly-vegetated areas, at vicinity of seagrass meadows.

The foraminiferal assemblage of the scleractinian floatstones suggests that coral fragments probably came from nearby inner-shelf patch reef frameworks or could represent sparse coral colonies within seagrass meadows. The few *in situ* coral bioconstructions observed in the B3 Népü Limestone Member suggest that they were probably relatively sparse on sea bottom of relatively small dimensions (meter-scale).

As a consequence, the biotic composition and the textural characters of the FA6 facies association suggest a deposition within the euphotic zone, in a relatively high energy environment which is extensively vegetated by seagrass meadows and colonized by sparse and small-sized coral bioconstructions. Additionally, the sub-rounded pebble lags which are interbedded within carbonate deposits are an additional evidence for the proximity of the ultramafic source in this mixed system and likely represent the reworking of fluvial outputs by waves and marine currents (Nemec & Steel, 1984).

### *FA7- Subaqueous distributary channel fills (Fig. 15)*

*Description:* in the proximal part of the B3 Népü Limestone Member, numerous conglomeratic channel-fills occur. They are particularly well-exposed on the Pindaï Peninsula, at the

southeastern extremity of the Wharf outcrops (Fig. 15A), and to the South of the *Baie des Sapins* (Fig. 15C). They cut into shallow water limestones and are 2 to 5 meters-thick and 15 to 30 meters-wide. At the Wharf outcrops, they are stacked into amalgamated channel complexes (Fig. 15A). Individual channel fills comprise well rounded, ultramafic pebbles-cobbles in a calcareous matrix and coarse-grained gravelly sandstones (Fig. 15B). The composite infill is organized into a fining upward, laterally accreting stack of inclined bedsets.

*Interpretation:* the interfingering of conglomerate and carbonate ramp deposits, the sharp nature of erosional surfaces and the normally graded infills strongly suggest that these conglomerates deposited in subaqueous distributary channels which formed in an alluvial-fan front setting, by erosional currents transporting material from the Kopéto and Boulinda massifs into a shallow-water carbonate inner ramp (e.g. Nemec & Steel, 1984). The lack of bidirectional current structure would rule out a tidal origin for such channels. Such channels can be regarded as the main feeders of the coarse terrigenous fraction present within the FA6 carbonate deposits (conglomeratic lags).

### *FA8- Carbonate-dominated tidal flat (Fig. 16)*

*Description:* at the Wharf outcrops and the Grimault Islet (see location Fig. 4), the base of the B3 Népü Limestone Member is marked by an alternation of marls and centimeter-thick beds of very fine-grained sandy to silty limestones with plant debris (Fig. 16A). Some of these silty marls intervals are entirely cut by vertical pneumatophore roots (Fig. 16C). Among such alternations, lithoclastic wackestone to packstone beds with fragments of echinoids and gastropods are observed. In addition, several thin layers with decimeter-scale well rounded and well sorted ultramafic pebbles in a calcareous muddy matrix are also identified (Fig. 16D). Finally, sandy intervals display large scale sigmoidal dunes prograding towards the SSW to SSE. Foresets have a 5° to 15° dip and bedforms extend over at least several tens of meters. These deposits consist

493 in medium-grained sandstones with floating granules, common bioturbation and erosional
494 topsets (Fig. 16B).
495
496 *Interpretation:* the alternation between marls and fine-grained sandstones with vegetal debris
497 and pneumatophore roots is seen as characteristic of a supratidal to intertidal environment
498 (Shinn, 1983). Pneumatophore roots are highly likely to evidence a supratidal swamp in a
499 tropical climate. Sigmoidal dunes are consistent with this interpretation and root traces and leaf
500 fragments suggest that they formed in a supra to intertidal environment such as tidal sand bars.
501 Conglomerates, in turn, would correspond to the terminal distributary channels of the alluvial-
502 fan system.
503
504

## 4.2 Vertical distribution of facies association in the S2 cores.

The contact between the Aquitanian Lower Nepoui Formation and Burdigalian Upper Nepoui Formation is not observable at Chapeau Chinois outcrop (Fig.7 in Maurizot et al., 2016), but the transition is continuously recorded at well S2 (Fig. 17A). This transition, between –104 m and –98 m, shows the top of Lower Népoui Formation (Aquitanian after Maurizot et al., (2016)), which is characterized by scleratinian floastones with a foraminiferal-algal packstone matrix. The uppermost Lower Népoui limestones display in that location a rich foraminiferal assemblage characterized by a regular occurrence of *Miogypsina, Heterostegina, Lepidocyclina, Sorites, Neorotalia, Cibicides, Elphidium* and discorbids (Fig. 17B). The mixture of epiphytic foraminifers such as *Sorites*, *Neorotalia, Cibicides, Elphidium*, discorbids and larger foraminifers such as *Miogypsina*, *Lepidocyclina* and *Heterostegina* within the underlying limestones are indicative of a euphotic to upper mesophotic depositional environment for the uppermost Lower Népoui Formation (Pomar et al., 2014).

Between –98 m to –92 m depth, the transition from the Lower Népoui limestones to the Upper Népoui basal sandstones is gradational, with a progressive increase in terrigenous clasts and a decrease in biogenic components (Fig. 17C). At the top of this interval, fine to medium-grained clean sandstones (FA4-FA5 facies associations) display parallel to cross laminations with common bioturbation. A coarsening upward trend is evidenced between –92 m to –83 m, with coarse- to medium-grained cross-bedded sandstones at the top. Constitutive elements primarily comprise weathered serpentinite grains as well ferricrete clasts. Additionally, the sandstones from the entire terrigenous interval (–98 m - –83 m) are strongly bioturbated and contain a low-diversified foraminiferal assemblage (mainly broken and likely transported *Miogypsina* and *Sorites*). The clean nature of the sand, the occurrence of cross-bedded beds and the associated ichnofacies (*Thalassinoides-Dactyloidites*) suggest a deposition in a shallow, subtidal, high-energy environment.

This terrigenous interval is overlain by the 80 meters-thick Népü Limestone Member (B3), that is partially karstified and pervasively dolomitized (Fig. 17D). This interval displays

karst features infilled with reddish clay-rich sediment. Such reddish infills likely correspond to reworked laterites of the post-Burdigalian Muéo Formation that unconformably overlay the Miocene series (Coudray, 1975; Paris, 1981; Sevin et al., 2014).

The significant dolomitization of this interval could be explained by the high Mg content of runoff water derived from weathered peridotite massifs in an area where mixing fresh and marine water are already prone to induce secondary dolomitization (Tucker and Wright, 1990).

Finally, both the uppermost Lower Népoui and lowermost Upper Népoui formation were deposited in shallow waters, within the euphotic to upper mesophotic environments. As a consequence the upward transition from a carbonate-dominated to a siliciclastic-dominated system is not accompanied by a major shift in paleowater depth.

# 5. DISCUSSION

## 5.1 Revised depositional model for the Burdigalian Upper Népoui mixed system

This study proposes a revised depositional model of the Burdigalian Upper Népoui formation. This constrained by seven synthetic logs, from S2 core data and 6 key outcrop sections (Fig. 18), which capture the architecture of this mixed carbonate-siliciclastic system and its evolution through time (Fig. 19).

Facies analysis and correlation of synthetic cross-sections suggest that alluvial fan and fluvial deposits (FA1, FA2 and FA3) evolve distally into tidally influenced nearshore sandstone deposits (FA4 and FA5) in only a few kilometers, in the lower part of the Upper Népoui formation (Fig. 18). Alluvial deposits are of restricted extension and the relatively sharp transition to marine deposits together with the lack of preserved floodplain deposits strongly suggest a fan delta depositional system (*sensu* Holmes, 1965). The good preservation of tidal deposits could also be

consistent with sedimentation occurring within a paleovalley (estuarine environment) or a lagoonal embayment (Dalrymple et al., 1992). However, the lateral continuity of facies associations along a 10 km-long transect (perpendicularly to a proximal-distal axis), between the Pindaï peninsula and the Beco Island (Fig. 18), favors a fan delta system developing on an unconfined continental shelf. During this stage, continental alluvial fan deposits (FA1, FA2 and FA3) would evolve laterally into a relatively wide and low-angle shelf (up to 5 km) where intertidal (FA4) and subtidal (FA5) terrigenous sedimentation occurs (Fig. 19A). In the S2 well, a relatively thin (< 20m) siliciclastic unit, composed of facies associations FA5 and FA4 progressively changes upward into carbonate ramp deposits (FA6). This transitional facies change suggests coeval terrigenous inputs and carbonate ramp sedimentation. Lateral transition between shallow-water carbonates and siliciclastic deposits is observed in the modern lagoon of New Caledonia where high fluvial discharges from peridotite massif watersheds (Garcin et al., 2013) are coeval with high carbonate productivity (Chevillon, 1992; Cabioch et al., 2008; Le Roy et al., 2019). Carbonate sedimentation in the B3 member is dominated by seagrass-related carbonate production (FA6), suggesting that the subtidal, euphotic shelf was extensively covered by seagrass meadows. In Pindaï and Grimault sections the upward vertical transition from terrigenous-dominated to carbonate-dominated sedimentation is characterized by the development of a carbonate-dominated unit deposited in tidal-flat and swamp environments (FA8). This suggests that tidal currents were able to import toward coastal environments (tidal flat and swamps) significant volume of carbonate sediment produced in subtidal seagrass environments. The interfingering of conglomerate-filled channels (FA7) within FA6 and FA8 carbonate deposits indicate that the coarse terrigenous fraction of the sediment was supplied by the alluvial fan through distributary channels cross-cutting the tidal flat and the subtidal seagrass meadows (Fig.19B). Similar conglomerate-filled feeder channels developing at the mouth of river courses and cross-cutting shallow-water mixed carbonate-siliciclastic deposits have been evidenced at the front of a Tortonian fan delta from the Vera Basin, Spain (Braga et al., 2001). These channels, which are not related to relative sea level falls and emersion of the shelf

(i.e. incised valley fills), have been shown to feed turbidite lobes in the basin. Similarly, in the Burdigalian Upper Népoui formation, conglomerate-filled channels cross-cutting seagrass deposits (FA8) are subquaeous and developed during an overall transgressive trend. As a consequence, the vertical and lateral evolution of facies within the Burdigalian Upper Népoui formation requires the definition of two distinct depositional models for the mixed carbonate-siliciclastic system: 1) a siliciclastic-dominated system, during relative sea level lowstand and/or early transgression, characterized by an extensive terrigenous intertidal and subtidal domain and by moderate seagrass carbonate production (Fig. 19A), 2) a carbonate-dominated ramp system, during later transgression and possibly relative sea level highstand, typified by extensive seagrass meadow development over the entire subtidal, euphotic domain (Fig. 19B). Distal equivalents in mesophotic to oligophotic environments are not observed in the current dataset.

## 5.2 Factors controlling the depositional architecture of the Upper Népoui Formation

The depositional environments recorded by the Burdigalian deposits of Népoui suggest significant creation of accommodation space as well as *in situ* changes of environmental conditions. During the Burdigalian, the onset of siliciclastic sediment deposition (B1 Pindaï Conglomerates and B2 Wharf Members) overlying the Aquitanian ramp is recorded in the S2 well by a progressive shift towards sandy terrigenous deposits with an upward decrease in carbonate components (Fig. 17). This transition marks the demise of the Aquitanian carbonate ramp, most likely due to a significant increase in water turbidity associated with the progradation of alluvial fans. This facies shift has been formerly interpreted by Maurizot et al. (2016) as resulting from a major forced regression driven by a tectonic uplift. However, the lack of subaerial exposure evidence and the lack of significant paleobathymetric gap between the top Aquitanian limestones (euphotic environment: 0–20m) and the base Burdigalian tidal sands in

S2 well do not support this interpretation of a forced regression at the Lower Népoui-Upper Népoui transition. The increase of detrital fluxes and transient decrease or demise of carbonate production during the Burdigalian in the Népoui area may result from other parameters such as: 1) an intensification of erosional and/or weathering processes on peridotite massifs due to climate changes or to gravitational collapses linked with the fault network structuring Grande Terre (Iseppi et al., 2018), or 2) an autocyclic lateral migration of a pre-existing alluvial fan system. The overall transgressive trend recorded in the Pindaï Peninsula by the upward succession from fluvial to intertidal and finally subtidal carbonate ramp deposits suggests that the Upper Népoui formation developed during a period of increasing accommodation space. Published eustatic curves indicate an overall increase of eustatic sea level up to 80 meters during the Burdigalian (Haq et al., 1987; Miller et al., 2005). Hence, eustatic variations may have largely controlled the creation of accommodation space which allowed the accumulation of 60 meters (outcrops of Pindaï Peninsula) to 100 meters (S2 well) of alluvial to shallow-water (shoreface sands and euphotic seagrass carbonates) deposits. This creation of accommodation space may also be linked to the collapse of the western margin driven by the post-obduction isostasic rebound of Grande Terre (Lagabrielle & Chauvet, 2008, Collot et al., 2017).

### 5.3 Seagrass and patch-reef carbonate production in high-terrigenous influx settings

A variety of carbonate-producing biota, including some large benthic foraminifera, coralline algae, echinoderms, molluscs, and corals, tolerate nearly continuous siliciclastic influx (e.g. Wilson, 2005; Novak et al., 2013; Santodomingo et al., 2015). The most distinctive character of the lower Miocene carbonate sedimentation of the Népoui system is the dominance of seagrass associated production, with also common occurrence of coral bioconstructions (meter-scale patches). Seagrass-related carbonate production has been shown to be highly tolerant to high terrigenous fluxes in various Cenozoic carbonate systems (e.g. Beavington-Penney et al., 2004;

Reuter et al., 2012; Brandano and Ronca, 2014; Tomas et al., 2016). In such settings, variations in terrigenous supplies modify the taxonomic composition of plant assemblages on sea bottom and therefore the morphology of phytal substrates for epiphytic foraminifers. In modern environments, the nature and composition of epiphytic communities have been shown to depend on the species of the seagrass substrate (e.g. Beavington-Penney et al., 2004; Perry et al., 2012) or more commonly to the nature of the phytal substrate (seagrass vs macro-algae: Fujita & Hallock, 1999 ; Benedetti & Frezza, 2016). Morphotypes of epiphytic foraminifers have been revealed to be useful to analyze the assemblage structure and provide criteria to infer different types of phytal substrates (Langer, 1993; Mateu-Vicens et al., 2010; 2014). Seagrasses are typically dominated by flat, discoidal foraminiferal morphotypes (A and SB morphotypes after Langer's (1993) classification, modified by Mateu-Vicens et al., 2014) since these foraminifers have long life cycles (at least one year) and require long lasting and flat substrates. In contrast, macroalgae, whose life span is shorter, are the substrate of smaller and robust foraminifers (morphotypes B and D) with shorter life cycles (Mateu-Vicens et al., 2010). The porcelaneous-dominated epiphytic association from Népoui is largely composed of SB morphotypes (flat and discoidals soritids, peneroplids) and likely reflects a dominant seagrass substrate. In contrast, the abundance of Neorotalia (morphotype B) in the calcarinid-dominated association would characterize environments significantly colonized by macroalgae.

Repeated changes in epiphytic foraminiferal associations (porcelaneous-dominated vs calcarinid (*Neorotalia*)-dominated) within the Népü limestone may therefore reflect changes through time and space of the nature of the phytal substrate which in turn can reflect variations in some environmental parameters such as turbidity or salinity. In modern tropical carbonate environments, the dominance of calcarinids has been shown to be related to the extensive development of macro-algae (Renema, 2010).

The Miocene seagrass skeletal association from Népoui is characterized by a high foraminiferal (52 % of the sand-grained skeletal fraction in average) and coralline algal content (33 %), and an extreme scarcity of *Halimeda* green algae. Such a bioclastic composition is consistent with the RA

(red-algal) foralgal seagrass assemblage (Brandano et al., 2019), which characterizes high density tropical to subtropical seagrass meadows. RA-foralgal seagrass-related association is reported from modern Mediterranean environments (Brandano et al., 2019) as well as from a variety of ancient tropical carbonate systems (e.g. Seeb Formation, Eocene, Oman: Beavington-Penney et al., 2004; Malampaya buildup, Philippines, Chattian to Burdigalian: Fournier et al., 2004, SE Spain, Messinian: Sola et al., 2013). In densely vegetated areas, particularly in the case of long-leaved seagrasses, oligophotic conditions prevail at sea bottom thus impeding the development of green algae and promoting in contrast coralline algae, which are known to be highly tolerant to low-light, oligo-mesotrophic conditions. Such an interpretation may explain the high coralline content and the scarcity of *Halimeda* of seagrass sediments in the Népoui seagrass-related sediment, but the oligophotic conditions at sea bottom can also result of relatively high-turbidity created by strong terrigenous discharges. As a consequence it can be suggested that in high-terrigenous settings, RA-foralgal associations may also occur in low to moderately dense seagrasses as a result of water turbidity.

Seagrass meadows have a significant effect on current velocity reduction, sediment trapping and decreasing resuspension of particles thus leading to a reduction of the turbidity in the water column (de Boer, 2007). The reduction of fine particle resuspension within seagrass meadows may have drastically limited the negative effect of water turbidity for the development of light-dependent biota such as symbiont-bearing foraminifers, coralline algae and corals.

Differential trapping of sediments within the seagrass meadow may lead to slightly raised sea bottom in vegetated areas (e.g. Pérès & Picard, 1964; Madsen et al., 2001; Fujita et al. 2015). Water flow and terrigenous influx are therefore likely to be directed toward the lower lying areas, thus reducing the risk of suffocation for filter-feeding biota living in the seagrass meadow. The coeval development of seagrass meadows and terrigenous sediment flows on the alluvial-fan front possibly also controls the aggrading nature (vertical stack) of the main distributary channel infills (Fig 15).

692 Additionally, scleractinian bioconstructions that form in turbid water under significant
693 terrigenous inputs, are common in the geological record (e.g. Sanders & Baron-Szabo, 2005) and
694 particularly in Cenozoic shallow-water sedimentary systems from the Indo-Pacific (e.g. Wilson,
695 2005; Novak et al., 2013; Santodomingo et al., 2015) and Mediterranean regions (Galloni et al.,
696 2001; Brandano et al., 2010, 2016; Mazzucchi &Tomassetti, 2011). This is consistent with the
697 common occurrence of coral fragments and in situ bioconstructions within the Lower and Upper
698 Népoui limestones. As evidenced from Miocene patch-reefs formed at the seaward margin of the
699 equatorial Mahakam Delta (Wilson, 2005), carbonate production and patch-reef development
700 may occur in turbid-water, delta-front areas during any phase of eustatic sea level.
701 The relative tolerance of seagrass ecosystems as well as small-scale coral patches environments
702 to high terrigenous influx may explain the significant development of ramp carbonate systems
703 with mixed foraminiferal and scleractinian production at the mouth of alluvial fan systems, in
704 tropical settings.
705
706

## 6. CONCLUSION

The Burdigalian carbonate ramp system of Népoui is a well-constrained example of seagrass-dominated and coral-bearing carbonate systems developing in high terrigenous influx setting and tropical climate.

(1) During the Burdigalian, the upward succession from the Pindaï conglomerate to the Népü Limestone member is the result of the retrogradation or lateral migration of a fan delta system passing laterally into a carbonate ramp, during a marine transgression. Despite this transgressive trend, the carbonate ramp received high-terrigenous influx as evidenced by small-scale conglomeratic channels that randomly incised the carbonate ramp.

(2) Post-obduction isostatic rebound resulted in an extensional tectonic regime and margin collapse that possibly favored the onset and preservation of terrigenous fan delta and carbonate ramp systems.

(3) Extensive development of seagrass meadows and potentially of macro-algae occurred in shallow, euphotic environments subject to high-terrigenous discharge. Phytal substrates induced by seagrass vs macro-algae colonization of sea bottom strongly controlled the nature of carbonate production and promoted the accumulation of foraminiferal-coralline algal sediments.

(4) Finally, the development of seagrass meadows has probably largely contributed to the preservation of a diverse and significant carbonate production in a context of strong terrigenous inputs, by reducing water turbidity and by limiting the risk of suffocation for filter-feeding biota.

The lateral and vertical variability of the Burdigalian carbonate ramp improves knowledge on the heterogeneity of potential hydrocarbon reservoirs in mixed carbonate-siliciclastic systems.

## ACKNOWLEDGEMENTS

This work was funded jointly by the Adecal Technopole and the Geological Survey of New Caledonia (SGNC) of the Department of Industry, Mines and Energy of New Caledonia (DIMENC).

We thank the Institute of Research for the Development (IRD) for the provision of core drilling material and the "*Diodon*" boat to access the islets. Special thanks to Mathieu Mengin (SGNC) and John Butcher (IRD) who conducted the core drilling work and Boris Marcaillou (GeoAzur), Samuel Tereua (IRD) and Miguel Clarque (IRD) for the boat travels to the islets that were sometimes difficult to approach.

# REFERENCES


**Aitchison, J. C., G. L. Clarke, S. Meffre, and D. Cluzel** (1995), Eocene arc-continent collision in New Caledonia and implications for regional Southwest Pacific tectonic evolution, *Geology*, **23**(2), p. 161-164.

**Allen, J. R. L.,** (1963), The classification of cross-stratified units with notes on their origin: *Sedimentology*, v. **2**, no. **2**, p. 93–114.

**Allen, J. R. L.,** (1983), Studies in fluviatile sedimentation: Bars, bar-complexes and sandstone sheets (low-sinuosity braided streams) in the brownstones (L. devonian), welsh borders, *Sedimentary Geology*, v. **33**, no. **4,** p. 237–293.

**Bassant, P., Van Buchem, F.S.P., Strasser, A., Görür, N.** (2005), The stratigraphic architecture and evolution of the Burdigalian carbonate-siliciclastic sedimentary systems of the Mut Basin, Turkey. *Sedimentary Geol,ogy* , v. **173**, 187–232.

**Bassi, D. Nebelsick, J.,** (2010). Components, facies and ramps: redefining Upper Oligocene shallow water carbonates using coralline red algae and larger foraminifera (Venetian area, northeast Italy). *Palaeogeography, Palaeoclimatology, Palaeoecology*, v. **295**, 258–280.

**Beavington-Penney, S.J., Wright, V.P., Woelkerling, W.J.**, (2004), Recognising macrophyte vegetated environments in the rock record: a new criterion using 'hooked' forms of crustose coralline red algae. *Sedimentary Geology*, v. 166, p.1–9.

**Belderson, R., Johnson, M., and Kenyon, N.,** (1982), Bedforms, *in* Stride, A.H (ed.), Offshore tidal sands, processes and deposits, *Chapman and Hall*., pp.27–57.

**Belperio, A. P.** (1983). Terrigenous sedimentation in the central Great Barrier Reef lagoon: a model from the Burdekin region. *BMR Journal of Australian Geology and Geophysics*, **8**, no. **3**, p.179–190.

**Benedetti, A, Frezza, V.** (2016) Benthic foraminiferal assemblages from shallow‐water environments of northeastern Sardinia (Italy, Mediterranean Sea). *Facies*, **62**:14.

**Blair, T. C.,** (1999), Cause of dominance by sheetflood vs. debris-flow processes on two adjoining alluvial fans, Death Valley, California, *Sedimentology*, v. **46**, no. **6**, p. 1015–1028.

**Blair, T. C., and McPherson, J. G.,** (1994), Alluvial fans and their natural distinction from rivers based on morphology, hydraulic processes, sedimentary processes, and facies assemblages, *Journal of Sedimentary Research*, v. **64**, no. **3a**, p. 450–489.

**Bluck, B. J.,** (1979), Structure of coarse grained braided stream alluvium, *Earth and Environmental Science Transactions of the Royal Society of Edinburgh*, v. **70**, no. **10–12**, p. 181–221.

**Braga, J.-C, Martín, J.M., Wood, J.L.,** (2001), Submarine lobes and feeder channels of redeposited, temperate carbonate andmixed siliciclastic-carbonate platform deposits (Vera Basin, Almería, southern Spain). *Sedimentology*, v. **48**, p. 99–116.

**Brandano, M., Frezza, V., Tomassetti, L., Pedley, M., Matteucci, R.,** (2009). Facies analysis and palaeoenvironmental interpretation of the Late Oligocene Attard Member (Lower Coralline Limestone Formation), Malta. *Sedimentology*, v. **56**, no. **4**, p. 1138–1158.

**Brandano M., Frezza V., Tomassetti L., Bosselini F. & Mazzucchi A**. (2010): Depositional model and paleodepth reconstruction of a coral-rich, mixed carbonate-siliciclastic system: the Burdigalian of Capo Testa (northern Sardinia, Italy). *Facies*, v. **56**, p. 433–444.

**Brandano, M., Ronca, S.,** (2014). Depositional processes of the mixed carbonate–siliciclasticrhodolith beds of the Miocene Saint-Florent Basin, northern Corsica. *Facies*, v. **60**, 73–90.

**Brandano M., Tomassetti, L., Frezza V.,** (2015). *Halimeda* dominance in the coastal wedge of Pietra di Finale (Ligurian Alps, Italy): The role of trophic conditions. *Sedimentary Geology*, v. **320**, 30-37.

**Brandano, M., Bosellini, F.R., Mazzucchi, A., Tomassetti**, L., (2016). Coral assemblages and bioconstructions adapted to the depositional dynamics of a mixed carbonate siliciclastic setting: the case study of the Burdigalian Bonifacio Basin (South Corsica). *Rivista Italiana di Paleontologia e Stratigrafia*, v. **122**, 37-52.

**Brandano, M., Tomassetti, L. Mateu Vicens, G., Gaglianone, G.,** (2019). The seagrass skeletal assemblage from modern to fossil and from tropical to temperate: Insight from Maldivian and Mediterranean examples. *Sedimentology*, v. **66**, p. 2268–2296.

**Cabioch, G., Correge, T., Turpin, L., Castellaro, C., and Recy, J.**, (1999), Development patterns of fringing and barrier reefs in New Caledonia (southwest Pacific), *Oceanologica acta*, v. **22,** no. **6**,p. 567–578.

**Cabioch, G., Montaggioni, L., Thouveny, N., Frank, N., Sato, T., Chazottes, V., Dalamasso, H., Payri, C., Pichon, M. and Sémah, A.-M.** (2008) The chronology and structure of the western New Caledonian barrier reef tracts. *Palaeogeography, Palaeoclimatology, Palaeoecology*, v. **268,** p.91–105.

**Cabioch, G., Recy, J., Jouannic, C., and Turpin, L.,** (1996). Contrôle climatique et tectonique de l'édification récifale en Nouvelle-Calédonie au cours du Quaternaire terminal, *Bulletin de la Société Géologique de France,* v. **167**, no. **6**, p. 729–742.

**Catuneanu, O.,** (2019). Model-independent sequence stratigraphy . *Earth-Science Reviews*, **188**, p. 312-88.

**Chaproniere, G.C.H.,** (1975). Palaeoecology of Oligo-Miocene Foraminifera, Australia. *Alcheringa* **11**, p. 37–58.

**Chevillon, C.,** (1992). Biosédimentologie du grand lagon nord de la Nouvelle-Calédonie, ORSTOM, Aix-Marseille II, 224 p.

**Cluzel, D.,** (1998). Le Flysch post-obduction de Népoui, un bassin transporté ? Conséquences sur l'âge et les modalités de l'obduction tertiaire en Nouvelle-Calédonie (Pacifique sud-ouest). *Comptes Rendus de l'Académie des Sciences – Series IIA – Earth and Planetary Science,* **v. 327**, no. **6**, p. 419–424.

**Cluzel, D., J. Aitchison, G. Clarke, S. Meffre, and C. Picard** (1994), Point de vue sur l'évolution tectonique et géodynamique de la Nouvelle-Calédonie (Pacifique, France), *Comptes Rendus de l'Académie des Sciences*, Série 2, **319**(6), p. 683-690.

**Cluzel, D., J. C. Aitchison, and C. Picard** (2001), Tectonic accretion and underplating of mafic terranes in the late Eocene intraoceanic fore-arc of New Caledonia (Southwest Pacific): geodynamic implications, *Tectonophysics*, **340**(1/2), p. 23-59.

**Cluzel, D., Bosch, D., Paquette, J. L., Lemennicier, Y., Montjoie, P., and Ménot, R. P.,** (2005). Late Oligocene post-obduction granitoids of New Caledonia: A case for reactivated subduction and slab break-off. *Island Arc,* v. **14,** no. **3**, p. 254–271.

**Cluzel, D., P. Maurizot, J. Collot, and B. Sevin** (2012), An outline of the geology of New Caledonia; from Permian-Mesozoic South-Gondwana active margin to Tertiary obduction and supergene evolution, Episodes, **35**(1), p. 72-86.

**Cluzel, D., Picard, C., Aitchison, J. C., Laporte, C., Meffre, S., and Parat, F.,** (1997), La nappe de Poya (ex-Formation des Basaltes) de Nouvelle-Calédonie (Pacifique sud-ouest): un plateau océanique campanien-paléocène supérieur obducté à l'Eocène supérieur, *Comptes Rendus de l'Académie des Sciences – Series IIA – Earth and Planetary Science,* v. **324**, p. 443–451.

**Collot, J., Geli, L., Lafoy, Y., Vially, R., Cluzel, D., Klingelhoefer, F., and Nouzé, H.,** (2008), Tectonic history of northern New Caledonia Basin from deep offshore seismic reflection: Relation to late Eocene obduction in New Caledonia, southwest Pacific. *Tectonics,* v. **27**, no. **6**., 20 p.

**Collot, J., Patriat, M., Etienne, S., Rouillard, P., Soetaert, F., Juan, C., Marcaillou, B., Palazzin, G., Clerc, C., Maurizot, P., Pattier, F., Tournadour, E., Sevin, B., and Privat, A.,** (2017). Deepwater Fold-and-Thrust Belt Along New Caledonia's Western Margin: Relation to Post-obduction Vertical Motions. *Tectonics*, v. **36**, no**. 10**, p. 2108–2122.

**Coudray, J.,** (1975), Recherches sur le Néogène et le Quaternaire marin de la Nouvelle-Calédonie. Contribution de l'étude sédimentologique à la connaissance de l'histoire géologique post-éocène, Thèse de Doctorat, Université des Sciences et Techniques du Languedoc, 446 p.

**Dalrymple, R. W., Zaitlin, B. A., and Boyd, R.,** (1992). Estuarine facies models; conceptual basis and stratigraphic implications. *Journal of Sedimentary Research,* v. **62**, no. **6**, p. 1130–1146.

**De Boer, W.F.**, (2007). Seagrass–sediment interactions, positive feedbacks and critical thresholds for occurrence: a review. *Hydrobiologia*, v. **591**, p. 5–24.

**Dubois, J., Launay, J., and Recy, J.,** (1974). Uplift movements in New Caledonia-Loyalty Islands area and their plate tectonics interpretation. *Tectonophysics*, v. **24**, no. **1**, p. 133–150.

**Eva, A.N**., (1980). Pre-Miocene seagrass communities in the Caribbean. *Palaeontology*, v. **23**, 231–236.

**Fabricius, K.E.,** (2005). Effects of terrestrial runoff on the ecology of corals and coral reefs: review and synthesis. *Marine Pollution Bulletin*, v. **50**, p. 125–146.

**Fournier, F., Montaggioni, L., and Borgomano, J.,** (2004). Paleoenvironments and high-frequency cyclicity from Cenozoic South-East Asian shallow-water carbonates: a case study from the Oligo-Miocene buildups of Malampaya (Offshore Palawan, Philippines), *Marine and Petroleum Geology*, v. **21,** no. **1**, p. 1–21.

**Fujita, K; Hallock, P** (1999). A comparison of phytal substrate preferences of Archaias angulatus and Sorites orbiculus in mixed macroalgal-seagrass beds in Florida Bay. *Journal of Foraminiferal Research*, v. **29**, no. 2, p. 143-151

**Fujita, K., Asami, R., Takayanagi, H., and Iryu, Y.** (2015) Carbonate sedimentation in seagrass beds on Ishigaki-jima, Ryukyu Islands, southwestern Japan. *Island Arc*, **24**, p. 263–279

**Gaina, C., Müller, D. R., Royer, J. Y., Stock, J., Hardebeck, J., and Symonds, P.,** (1998). The tectonic history of the Tasman Sea: a puzzle with 13 pieces. J*ournal of Geophysical Research: Solid Earth* (1978–2012), v. **103**, no. **B6**, p. 12413–12433.

**Galloni F., Cornee J.J., Rebelle M. & Ferrandini M.** (2001) Sedimentary anatomies of early Miocene coral reefs in South Corsica (France) and South Sardinia. *Géologie Mediterranéenne*, v. **28**, 73-77.

**Garcin, M., Baills, A., Le Cozannet, G., Thomas, T., Auboin, A. L., and Sauter, J.,** (2013). Pluri-decadal impact of mining activities on coastline mobility of estuaries of New Caledonia (South Pacific), *Journal of Coastal Research*, v. **65**, p. 494–499.

**Gubler, Y., and Pomeyrol, R.,** (1948), Existence de Néogène marin en Nouvelle-Calédonie. *Comptes Rendus de l'Académie des Sciences,* v. **226**, p. 1292–1293.

**Haig, D.W., Smith, M.G., Riera, R., Parker, J.H.,** (2020). Widespread seagrass meadows during the Early Miocene (Burdigalian) in southwestern Australia paralleled modern seagrass distributions. *Palaeogeography, Palaeoclimatology, Palaeoecology*, v. **555**, 109846.

**Hallock, P., and Glenn, E. C.**, (1986). Larger Foraminifera: A Tool for Paleoenvironmental Analysis of Cenozoic Carbonate Depositional Facies. *Palaios*, v. **1**, no. **1**, p. 55–64.

**Hallock, P., Sheps, K., Chapronière, G., Howell, M.,** (2006). Larger benthic foraminifers of the Marion Plateau, northeastern Australia (ODP Leg 194): comparison of faunas from bryozoan (Sites 1193 and 1194) and red algal (Sites 1196–1198) dominated carbonate platforms. In: Anselmetti, F.S., Isern, A.R., Blum, P., Betzler, C. (Eds.), *Proceedings ODP, Scientific Results*, pp. 1–31.

**Haq, B. U., Hardenbol, J., and Vail, P. R.,** (1987). Chronology of Fluctuating Sea Levels Since the Triassic. *Science*, v. **235**, no. **4793**, p. 1156–1167.

**Harper, B., Puga-Bernabéu, A., Droxler, A. W., Webster, J. M., Gischler, E., Tiwari, M., Lado-Insua, T., Thomas, A., L., Morgan, S., Luigi, J., and Rohl, U.,** (2015). Mixed carbonate–siliciclastic sedimentation along the Great Barrier Reef upper slope: A challenge to the reciprocal sedimentation model. *Journal of Sedimentary Research*, v. **85**, no. **9**, p. 1019–1036.

**Hernández-Arana, H., Vega-Zepeda, A.A., Ruíz-Zárate, M.A., Falcón-Álvarez, L.I., López-Adame, H., Herrera-Silveira, J., Kaster, J.,** (2015) Transverse coastal corridor: from freshwater lakes to coral reefs ecosystems . In: Islebe, G.A., Calmé, S., León-Cortés J.L., et Schmook, B., (Eds.), Biodiversity and Conservation of the Yucatán Peninsula, *Cham: Springer International Publishing*, pp. 355-376.

**Holmes, A.,** (1965). Principles of physical geology, 2nd ed, Thomas Nelson, London, 730 pp.

**Iseppi, M., Sevin, B., Cluzel, D., Maurizot, P., and Le Bayon, B.,** (2018). Supergene Nickel ore deposits controlled by gravity-driven faulting and slope failure, peridotite nappe, New Caledonia, *Economic Geology*, v. **113**, no. **2**, p. 531–544.

**James, N.P., and Bone, Y.** (2007). A Late Pliocene–Early Pleistocene, inner-shelf, subtropical, seagrass-dominated carbonate: Roe Calcarenite, Great Australian Bight, Western Australia. *Palaios*, v. **22**, p. 343–359.

**van Katwijk, M.M., Meier, N., van Loon, R., van Hove, E., Giesen, W., van der Velde, G., den Hartog, C.,** (1993). Sabaki River sediment load and coral stress: correlation between sediments and condition of the Malindi-Watamu reefs in Kenya (Indian Ocean): *Marine Biology*, v. **117**, p. 675–683.

**Kerans, C., and Tinker, S. W.** (1999). Extrinsic stratigraphic controls on development of the Capitan reef complex. *SEPM special publication,* no. **65,** p. 15–36

**Lafoy, Y., Dupont, J., Missegue, F., Le Suave, R., and Pautot, G.,** (1995), Effets de la collision « ride des Loyauté-arc des Nouvelles-Hébrides » sur la terminaison sud de l'ensemble « Nouvelle-Calédonie-Loyauté ». *Comptes Rendus de l'Académie des Sciences – Series IIA – Earth and Planetary Science,* **320**, p. 1101–1108.

**Lagabrielle, Y., and Chauvet, A.,** (2008). The role of extensional tectonics in shaping Cenozoic New-Caledonia, *Bulletin de la Société Géologique de France*, v. **179**, no. **3**, p. 315–329.

**Langer, M. R.,** (1993), Epiphytic foraminifera, *Marine Micropaleontology*, v. **20**, p. 235–265.

**Le Roy, P., Jorry, S., Jouet, G., Ehrhold, A., Michel, G., Gautier, V. and Guérin, C.** (2019). Late Pleistocene evolution of the mixed siliciclastic and carbonate southwestern New Caledonia continental shelf/lagoon. *Palaeogeography, Palaeoclimatology, Palaeoecology,* v. **514**, p. 502–521.

**Lukasik, J.J., James, N.P., McGowran, B., and Bone, Y.** (2000): An epeiric ramp: low-energy, cool-water carbonate facies in a Tertiary inland sea, Murray Basin, South Australia. *Sedimentology,* v. **47**, p. 851–881.

**Madsen, J. D., P. A. Chambers, W. F. James, E. W. Koch, and D. F. Westlake,** (2001). The interaction between water movement, sediment dynamics and submersed macrophytes. *Hydrobiologia*, v. **444**, p. 71–84.

**Mateu-Vicens, G., Hallock, P., Brandano, M.,** (2008). A depositional model and paleoecological reconstruction of the Lower Tortonian distally steepened ramp of Menorca (Balearic Islands, Spain). *Palaios*, v. **23**, 465–481.

**Mateu-Vicens, G., Hallock, P., Brandano, M.** (2009). Test shape variability of Amphistegina D'Orbigny 1826 as a paleobathymetric proxy: application to two Miocene examples. In: Demchuk, T., Gary, A. (Eds.), Geologic Problems Solving with Microfossils. *SEPM Spec. Publ*., pp. 67 - 82

**Mateu-Vicens, G., Box, A., Deudero, S., and Rodriguez, B.,** (2010). Comparative analysis of epiphytic foraminifera in sediments colonized by seagrass Posidonia oceanica and invasive macroalgae Caulerpa spp. *Journal of Foraminiferal Research*, v. **40**, p. 134–147.

**Mateu-Vicens, G., Brandano, M., Gaglianone, G., Baldassarre, A.,** (2012). Seagrass-meadow sedimentary facies in a mixed siliciclastic–carbonate temperate system in the Tyrrhenian Sea (Pontinian Islands, Western Mediterranean). *Journal of Sedimentary Research*, v. **82**, p. 451–463.

**Mateu-Vicens, G., Khokhlova, A., and Sebastián-Pastor, T.,** (2014). Epiphytic foraminiferal indices as bioindicators in Mediterranean seagrass meadows, *Journal of Foraminiferal Research*, v. 4**4**, p. 325–339.

**Maurizot, P., Cabioch, G., Fournier, F., Leonide, P., Sebih, S., Rouillard, P., Montaggioni, L., Collot, J., Martin-Garin, B., Chaproniere, G., Braga, J. C., and Sevin, B.,** (2016). Post-obduction carbonate system development in New Caledonia (Népoui, Lower Miocene). *Sedimentary Geology,* v. **331**, p. 42–62.

**Maurizot, P., & Vendé-Leclerc, M.** (2009). New Caledonia geological map, scale 1/500000. *Direction de l'industrie, des mines et de l'énergie–Service de la géologie de Nouvelle-Calédonie, Bureau de recherches géologiques et minières.*

**Mazzucchi, A., Tomassetti, L. (2011),** Coral bioconstruction in a Burdiagalian mixzs siliciclastic-carbonate coastal system (Cala, Paraguano, Corsica)*, Journal of Mediterranean Earth Sciences*, v. **3**, p.15-23.

**McNeill D.F., Cunningham K.J., Guertin L.A., and Anselmetti F.S.,** (2004). Depositional themes of mixed carbonate-siliciclastics in the South Florida Neogene: application to ancient deposits. In: Integration of outcrop and modern analogs in reservoir modeling. *Am. Ass. Pet. Geol. Mem*., v. **80**, p. 23–43.

**McNeill, D.F., Janson, X., Bergman, K.L., and Eberli, G.P.,** (2010). Belize: A Modern Example of a Mixed Carbonate-Siliciclastic Shelf. In: Westphal, H., Riegl, B., and Eberli, G.P., (Eds.) Carbonate depositional systems: assessing dimensions and controlling parameters: the Bahamas, Belize and the Persian/Arabian Gulf, *Dordrecht: Springer Netherlands,* pp. 81-143.

**Miall, A. D.,** (1977). A review of the braided-river depositional environment. *Earth-Science Reviews,* v. **13**, no. **1**, p. 1–62.

**Miall, A. D.,** (1985). Architectural-element analysis: A new method of facies analysis applied to fluvial deposits, *Earth-Science Reviews*, v. **22**, no. **4**, p. 261–308.

**Miller, K. G., Kominz, M. A., Browning, J. V., Wright, J. D., Mountain, G. S., Katz, M. E., Sugarman, P. J., Cramer, B. S., Christie-Blick, N., and Pekar, S. F.,** (2005). The Phanerozoic Record of Global Sea-Level Change. *Science*, v. **310**, no. **5752**, p. 1293–1298.

**Montaggioni, L. F., Cabioch, G., Thouveny, N., Frank, N., Sato, T., and Sémah, A.-M.,** (2011). Revisiting the Quaternary development history of the western New Caledonian shelf system: From ramp to barrier reef. *Marine Geology*, v. **280**, no. **1**, p. 57–75.

**Moretti, I., and Turcotte, D.,** (1985). A model for erosion, sedimentation, and flexure with application to New Caledonia, *Journal of geodynamics*, v. **3**, no. **1**, p. 155–168.

**Mortimer, N., Campbell, H. J., Tulloch, A. J., King, P. R., Stagpoole, V. M., Wood, R. A., Rattenbury, M. S., Sutherland, R., Adams, C. J., Collot, J., and Seton, M.,** (2017), Zealandia: Earth's Hidden Continent. *The Geological Society of America*, v. 27, p. 27-35.

**Nemec, W., Steel, R.J.,** (1984), Alluvial and coastal conglomerates: Their significant features and some comments on gravelly mass flow deposits. In: Koster, E. H., and Steel, R. J. (Eds.), Sedimentology of Gravels and Conglomerates. *Canadian Society of Petroleum Geologists Memoir,* v. **10**, pp. 1–31.

**Novak, V., Santodomingo, N., Rösler, A., Di Martino, E., Braga, J.C., Taylor, P.D., Johnson, K.G. and Renema, W.** (2013) Environmental reconstruction of a late Burdigalian (Miocene) patch reef in deltaic deposits (East Kalimantan, Indonesia). *Palaeogeography, Palaeoclimatology, Palaeoecology*, v. **374**, p. 110–122.

**Novak, V., and Renema, W.,** (2015). Larger foraminifera as environmental discriminators in Miocene mixed carbonate-siliciclastic systems. *Palaios*, v. **30**, p. 40–52.

**Olivier, N., Carpentier, C., Martin-Garin, B., Lathuilière, B., Gaillard, C., Ferry, S., Hantzpergue, P., and Geister, J.** (2004). Coral-microbialite reefs in pure carbonate versus mixed carbonate-siliciclastic depositional environments: the example of the Pagny-sur-Meuse section (Upper Jurassic, northeastern France). *Facies,* v. **50**, p. 229–255.

**Orpin, A. R., Brunskill, G.J., Zagorskis, I., and Woolfe, K. J.,** (2004). Patterns of mixed siliciclastic-carbonate sedimentation adjacent to a large dry-tropics river on the central Great Barrier Reef shelf, Australia. *Australian Journal of Earth Sciences,* v. **51**, no. **5**, pp. 665-683.

**Page, M.C., Dickens, G.R., and Dunbar, G.B.,** (2003). Tropical view of Quaternary sequence stratigraphy: Siliciclastic accumulation on slopes east of the Great Barrier Reef since the Last Glacial Maximum. *Geology*, v. **31**, no **11**, p. 1013–1016.

**Paquette, J.-L., and Cluzel, D.,** (2006). U–Pb zircon dating of post-obduction volcanic-arc granitoids and a granulite-facies xenolith from New Caledonia. Inference on Southwest Pacific geodynamic models. *International Journal of Earth Sciences,* v. **96**, no. **4**, p. 613–622.

**Paris, J. P.,** (1981). Géologie de la Nouvelle-Calédonie, Un essai de synthèse, *Mémoire du BRGM*, v. **113**, Orléans, France.

**Pérès, J.M. and Picard, J.** (1964) Nouveau Manuel de Bionomie benthique de la mer Méditerranée. *Rec. Trav. Stat. Mar. Endoume*, **3**, p. 1–137.

**Perry, C.T., Smithers, S.G., Gulliver, P., and Browne, N.K.,** (2012). Evidence of very rapid reef accretion and reef growth under high turbidity and terrigenous sedimentation. *Geology*, v. **40**, p. 719–722.

**Pomar, L., Mateu-Vicens, G., Morsilli, M., and Brandano, M.,** (2014), Carbonate ramp evolution during the Late Oligocene (Chattian), Salento Peninsula, southern Italy: *Palaeogeography, Palaeoclimatology, Palaeoecology,* v. **404**, p. 109-132.

**Posamentier, H. W., and Walker, R. G.,** (2006). Facies Models Revisited. *SEPM Society for Sedimentary Geology, Special publication,* v. **84.**

**Reich, S., Wesselingh, F.P., and Renema, W.,** (2014). A highly diverse molluscan seagrass fauna from the early Burdigalian (early Miocene) of Banyunganti (south-central Java, Indonesia). *Ann. Nat. Hist. Mus. Wien. Ser. A*, v. **116**, p. 5–129.

**Reich, S., Di Martino, E., Todd, J.A., Wesselingh F.P and Renema, W.** (2015) Indirect paleo-seagrass indicators (IPSIs): *A review. Earth-Sci. Rev.,* **143**, p. 161–186.

**Renema, W.** (2003) Larger foraminifera on reefs around Bali (Indonesia). *Zoologische Verhandelingen Leiden,* **345**, p. 337-366.

**Renema, W. (2005)** Depth estimation using diameter–thickness ratio in larger benthic foraminifera, *Lethaia,* v. **38**, p. 137–141.

**Renema, W.** (2010) Is increased calcarinid (foraminifera) abundance indicating a larger role for macro-algae in Indonesian Plio-Pleistocene coral reefs? *Coral Reefs*, **29**, p. 165-173.

**Reuter, M., Piller, W.E., Harzhauser, M., Kroh, A., Rögl, F., Coric, S.,** (2011). The Quilon Limestone, Kerala Basin, India: an archive for Miocene Indo-Pacific seagrass beds. *Lethaia*, v. **44**, 76–86.

**Reuter, M., Piller, W.E., and Ehrart, C.** (2012). A Middle Miocene carbonate platform under silici-volcaniclastic sedimentation stress (Leitha Limestone, Styrian Basin, Austria) — Depositional environments, sedimentary evolution and palaeoecology. *Palaeogeography, Palaeoclimatology, Palaeoecology*, v. **350-352,** p. 198–211.

**Reynaud, J.-Y., and Dalrymple, R. W.,** (2012). Shallow-Marine Tidal Deposits, in: Davis R. A., and Dalrymple, R. W., eds., Principles of Tidal Sedimentology, *Dordrecht, Springer Netherlands*, p. 335–369.

**Rigolot, P., and Pelletier, B.,** (1988). Tectonique compressive récente le long de la marge ouest de la Nouvelle-Calédonie: résultats de la campagne ZOE 400 du N/O Vauban (mars 1987): *Comptes rendus de l'Académie des sciences. Série 2, Mécanique, Physique, Chimie, Sciences de l'univers, Sciences de la Terre,* v. **307**, no. **2**, p. 179–184.

**Rogers, C.S., (1990),** Responses of coral reefs and reef organisms to sedimentation. *Marine Ecology Progress Series*, v. **62**, p. 185–202.

**Ryan-Mishkin, K, Walsh, J. P., Corbett, D. R. , Dail, M. B., and Nittrouer, J. A.,** (2009). Modern Sedimentation in a Mixed Siliciclastic-Carbonate Coral Reel Environment, La Parguera, Puerto Rico. *Caribbean Journal of Science*, v. **45,** no.2–3, p. 151–167.

**Sanders, D., and Baron-Szabo, R. C.,** (2005). Scleractinian assemblages under sediment input: their characteristics and relation to the nutrient input concept. *Palaeogeography, Palaeoclimatology, Palaeoecology,* v. **216**, no.**1**, p. 139–181.

**Santodomingo, N., Novak, V., Pretkovic, V., Marshall, N., Di Martino, E., Giudice Capelli, E., Rosler, A., Reich, S., Braga, J.C., Renema, W. and Johnson, K.G.** (2015) A diverse patch reef from turbid habitats in the middle miocene (East Kalimantan, Indonesia). *Palaios*, v. **30,** p. 128–149.

**Sevin, B., Cluzel, D., Maurizot, P., Ricordel - Prognon, C., Chaproniere, G., Folcher, N., and Quesnel, F.,** (2014). A drastic lower Miocene regolith evolution triggered by post obduction slab break-off and uplift in New Caledonia. *Tectonics*, v. **33**, no. **9**, p. 1787–1801.

**Silver, B.A., and Robert G.T.,** (1968). Permian Cyclic Strata, Northern Midland and Delaware Basins, West Texas and Southeastern New Mexico1. *AAPG Bulletin*, v. **53**, no. **11**, p. 2223-2251.

**Shinn, E. A.,** (1983). Tidal flat environment, Carbonate depositional environments. *American Association of Petroleum Geologists*, v. **33**, p. 171–210.

**Snedden, J. W., and Dalrymple, R. W.,** (1999), Modern shelf sand ridges: from historical perspective to a unified hydrodynamic and evolutionary model: *SEPM Society for Sedimentary Geology, Special publication*, v. **64**, p. 13–28

**Snedden, J. W., Kreisa, R. D., Tillman, R. W., Culver, S. J., and Schweller, W. J.,** (1999). An expanded model for modern shelf sand ridge genesis and evolution on the New Jersey Atlantic shelf. *SEPM Society for Sedimentary Geology*, *Special publication*, v. **64**, p. 147–164.

**Sola, F., Braga, J.C. and Aguirre, J.** (2013) Hooked and tubular coralline algae indicate seagrass beds associated to Mediterranean Messinian reefs (Poniente Basin, Almería, SE Spain). *Palaeogeogr. Palaeoclimatol. Palaeoecol.,* **374,** p. 218–229.

**Trescases, J. J.,** (1975). L'évolution géochimique supergène des roches ultrabasiques en zone tropicale : formation des gisements nickélifères de Nouvelle-Calédonie. *Mémoires ORSTOM*, v. **78**, 280 p.

**Tomás, S., Gianluca, F., Bömelburg, E., Zamagni, J., Perrin, C., Mutti M.,** (2016). Evidence for seagrass meadows and their response to paleoenvironmental changes in the early Eocene (Jafnayn Formation, Wadi Bani Khalid, N Oman). *Sedimentary Geology*, v. **341**, pp. 189-202.

**Tomassetti, L., Bosellini, F.R., Brandano, M**., (2013). Growth and demise of a coral bioconstruction on a granite rocky substrate (Bonifacio basin, southeastern Corsica). *Facies*, v. **59**, 703-716.

**Tomassetti, L., Benedetti, A., Brandano, M.,** (2016). Middle Eocene seagrass facies fromApennine carbonate platforms (Italy). *Sedimentary Geology*, v. **335**, 136-149.

**Tucker, M.E. and Wright, V.P.** (1990) Carbonate sedimentology. *Blackwell scientific publications.* Oxford, pp. 482.

**Uchman, A. and Pervesler, P.** (2007), Palaeobiological and palaeonvironmental significance of the Pliocene trace fossilDactyloidites peniculus. *Acta Palaeontologica Polonica* v. **52**, no **4** p.799–808.

**Vigorito M., Murru M., Simone L** .(2012). Carbonate production in rift basins: models for platform inception, growth and dismantling and for shelf to basin sediment transport, Miocene Sardinia Rift Basin, Italy. In: M. Mutti, W. Piller and C. Betzler (Eds.) Carbonate Systems during the Oligocene–Miocene Climatic Transition, *IAS Special Publication*, v. **42**, 257–282.

**Willis, B. J., Bhattacharya, J. P., Gabel, S. L., and White, C. D.,** (1999). Architecture of a tide‐influenced river delta in the Frontier Formation of central Wyoming, USA. *Sedimentology*, v. **46**, no. **4**, p. 667–688.

**Wilson, J. L.,** (1967). Cyclic and Reciprocal Sedimentation in Virgilian Strata of Southern New Mexico. *GSA Bulletin*, v. **78,** no. **7**, p. 805–818.

**Wilson, M.E.J.** (2005). Development of equatorial delta-front patch reefs during the Neogene, Borneo. *J. Sediment. Res.*, v. **75**, p. 114–133.

**Zeller, M., Verwer, K., Eberli, G. P., Massaferro, J. L., Schwarz, E., and Spalletti, L.,** (2015). Depositional controls on mixed carbonate–siliciclastic cycles and sequences on gently inclined shelf profiles. *Sedimentology*, **v. 62**, no. **7**, p. 2009–2037.

# FIGURE AND TABLE CAPTIONS

**Figure 1:** Simplified geological map of New Caledonia (modified after Maurizot & Vendé-Leclerc, 2009) with location of the study area, western limit of obducted peridotites, drilling sites on the quaternary barrier reefs (Coudray, 1975; Cabioch et al., 2008; Montagionni et al., 2011), together with map extent of the Deep-Water Fold and Thrust Belt of the western margin of New Caledonia (DWFTB, Collot et al., 2017). See text for details of these features.

**Figure 2**: (A) Geological map of the Népoui are modified from Maurizot & Vendé-Leclerc (2009), (B) cross section through the Kopeto massif and the Népoui miocene outcrops. The Lower Miocene mixed carbonate-siliciclastic system overlies unconformably the Eocene Népoui Flysch and the Poya Terrane on the western Caledonian margin. The Peridotite Nappe structurally overlies the Poya Terrane and the Nepoui Flysch.

**Figure 3:** Synthetic sedimentary log combining observations from the S4 well and outcrop sections. The Lower Miocene mixed system is composed of the Lower Népoui Formation (Aquitanian) and the Upper Népoui Formation (Burdigalian) dated by biostratigraphic analysis and strontium isotope measurements (Maurizot et al., 2016). Both formations are divided into three members A1 to A3 and B1 to B3 characterizing respectively a carbonate ramp and a mixed inner ramp delta system.

**Figure 4:** Location map of dataset used in this study. See location on Fig 1 and 2.

**Figure 5:** Description, sedimentary processes and summary depositional environment interpretation of the different facies associations of the Upper Népoui Formation (Burdigalian).

**Figure 6:** Proximal alluvial fan (FA1)

**A.** Massive, sandy matrix supported, poorly sorted conglomerate of the NE Pindaï Peninsula.

**B.** Altered serpentinite pebbles with silicified cortex and greenish sands.

**C.** Large block of dolerite that reach a diameter of 1 m.

**D.** Gravelly sandstones with faint trough cross-bedding highlighted by gravels and pebbles.

**E**. "Piste de roulage" outcrop (NW Muéo Peninsula) showing the unconformity between the Népoui Flysch (Priabonian) and the Upper Népoui Formation (Burdigalian) (see location on Fig.4).

**F.** Miocene conglomerates of the Upper Népoui Formation organized in two normally graded sequences as shown on the sedimentological section.

**Figure 7:** Distal alluvial fan (FA2)

**A.** Oblique bedded conglomerates that vertically evolve into trough cross-bedded sandstones capped by a planar abandonment surface.

**B.** Meter scale oblique bedsets showing an apparent progradation towards the SSW.

**C.** Red to greenish-red trough cross-bedded sandstones with root traces and iron oxide concretions

**D.** Silicified wood pieces.

**Figure 8:** Fluvial channel fills (FA3)

**A.** Interpretation of the depositional architecture of two erosional channels in the northern part of the Didot Islet (see location in Fig.4)

**B.** Conglomeratic channel fill

**C.** Conglomerates with large pebbles within a coarse to very coarse-grained sandy matrix organized in graded beds with erosional trough-shaped bases.

**D.** Large silicified wood trunk.

**Figure 9:** Tidal sands (FA4)

**A.** Small sigmoidal dunes showing tidal bundling and small scale trough-cross ripples between lamina sets

**B.** Herring-bone cross-bedding

**C.** Gravel and pebbles lags within a carbonate muddy matrix

**D.** Greenish coarse to medium-grained cross-bedded sandstones.

**E.** Thin section from the S2 well cores (85.6 m depth) showing altered serpentinite grains with radial fibrous cement and drusy cement.

**Figure 10:** Subtidal sands (FA5)

**A.** Fine-grained bioturbated sandstones with planar laminations and small-scale ripples

**B.** Isolated unidirectional ripples

**C.** *Dactyloidites peniculus* burrows in fine-grained sandstones

**D.** Fine-grained bioturbated and laminated sandstones.

**Figure 11:** Subtidal, seagrass related low-angle carbonate ramp (FA6)

**A.** Outcrop of the southern part of Grimault Islet (see location Fig. 4).

**B.** Focus on the southern part of Grimault Islet outcrop that shows foraminiferal-coralline algal packstone-grainstone facies.

**C.** Calcitic tubes are sparsely distributed over carbonate ramp deposits. They could be interpreted as tube worms.

**D.** Isolated corals and lags of ultramafic sub-angular pebbles and cobbles in a carbonate matrix.

**E.** Thin section from the S2 well core (41.25 m depth) showing two types of dolomite crystals: clear large rhomboidal crystals and small rhomboidal crystals with cloudy centers.

**F.** Karstified and dolomitized facies of the Nepü Member from S2 well cores (see location on Fig.4). Karst features and fractures are filled by mustard yellow clay, carbonate fragments and impregnated red mud.

**G.** Small-sized *in situ* coral bioconstructions embedded within coral floatstones and foraminiferal-coraline algal packstones-grainstones.

**Figure 12:** Simplified logs of the nine shallower drilled boreholes of the Pindaï Peninsula and Grimault Islet (see location Fig.4). Stars represent the locations of the thin sections.

**Figure 13:** Seagrass-related carbonate microfacies from the Burdigalian of Népoui (FA6) (see location of thin sections on Figure 12):

**A.** Foraminiferal-coralline algal packstone with abundant disk-shaped soritids (*Sor.*) and miliolids including *Austrotrillina* (*Austr.*). Grimault Island, well GR07, depth: 11.10 m.

**B.** Foraminiferal-coralline algal packstone with disk-shaped soritids (*Sor.*), small rotalids (*Rot.*), Halimeda (*Hal.*), articulated coralline algae (ARA), Planorbulina (Plan.) and lithoclasts (*Lith.*). Pindaï Peninsula, well 99N014, depth: 27.80m;

**C.** Foraminiferal-coralline algal packstone with disk-shaped soritids (*Sor.*), *Austrotrillina* (*Austr.*), the alveolinid Flosculinella (*Alv.*), articulated coralline algae (ARA) and Small miliolids (Mil.) Pindaï Peninsula, well 96N004, depth: 1.50m;

**D.** Foraminiferal-coralline algal packstone with small rotalids (*Neorotalia*) (Rot.), articulated coralline algae (ARA) and lithoclasts (*Lith.).* Pindaï Peninsula, well 99N014, depth: 27.80m;

**E.** Foraminiferal-coralline algal packstone with encrusting formainifers Victoriellids (*Vict.*), *Gypsina* (*Gyps.)* and small rotalids (*Rot.*). Pindaï Peninsula, well 96N002, depth: 11.10m;

**F.** Foraminiferal-coralline algal grainstone with disk-shaped soritids (*Sor.*), rotalids (*Rot.*), the alveolinid Flosculinella (*Alv.*) and articulated coralline algae (ARA). Grimault Island, well GR07.

**Figure 14:** Skeletal composition of the sand-grained skeletal fraction of seagrass-related carbonates (FA6) using point counting on thin-sections.

**Figure 15:** Subaqueous distributary channel fills (FA7).

**A.** The Wharf outcrop (see location Fig.4) showing a channel complex incising inner carbonate ramp and tidal flat deposits.

**B.** Close-up on carbonate matrix-supported conglomerates that fill channels.

**C.** The *Baie des Sapins* outcrop (see location Fig. 4) displays meter-scale isolated channels incising into carbonate ramp deposits.

**Figure 16:** Carbonate-dominated tidal flat deposits (FA8)

**A.** Marls interbedded with very fine-grained sandstones with plant debris.

**B.** Oblique sets of very bioturbated gravelly sandstones with truncated topsets.

**C.** Marls interbedded with very fine-grained sandstones and lithoclastic limestones intersected by pneumatophores roots.

**D.** Lag of well-sorted ultramafic pebbles in a carbonate matrix.

**Figure 17:** (A) Synthetic sedimentary log of S2 well (scale 1/500) (see location Fig.4). (B). Top of Lower Népoui Formation (Aquitanian), between -104 and -98 m, characterized by scleratinian floastones with a foraminiferal-algal grainstone-packstone matrix containing miogypsinids (*miog*.) and articulated coralline algae (*ARA*) (C). The lower part of the Upper Nepoui Formation (Burdigalian), between -98 to -83 m, characterized by fine to coarse-grained sandstones coarsening upward (FA4-FA5) that contain weathered serpentinite grains (Litho.), ferricrete clasts and few benthic foraminifers (*miog*.: miogypsinids). D. Népü Limestone Member (B3), between -80 to 0 m, showing pervasive karstification and laterite mud (*lm*) infills on cores. The thin section (-103 m) exhibit significant dolomitization features with few preserved bioclasts (RA: coralline algal fragments)

**Figure 18:** Synthetic sedimentary sections (scale: 1/500) revealing the frontal and lateral facies variability of the Upper Népoui Formation (Burdigalian).

**A.** Longitudinal profile within the proximal-distal sections of Muéo Peninsula, Pindaï-Wharf and Pindaï S2 core sections.

**B.** Lateral profile across the Burdigalian mixed system with the Pindaï- Wharf, Grimault, Didot, Longue and Beco sections.

**Figure 19:** Depositional models for the mixed carbonate-siliciclastic system of Népoui (Burdigalian). (A) The burdigalian mixed system is first dominated by short alluvial fan deposits that laterally evolve distally into tidally influenced nearshore sandstone deposits and towards shallow water carbonate dominated by seagrass-related biota and corals derived from small-sized bioconstructions, and (B) is then overlain by seagrass-related carbonate ramp cut by several small-scale conglomerate channels.

**Table 1:** Skeletal composition of the sand-sized fraction (in %) of FA6 limestones (seagrass-related facies association) from point counting on thin-sections. The location of wells and outcrop samples is reported on Figure 4. Texture code: P=Packstone; G=Grainstone; FP: floatstone with packstone matrix. Foraminiferal assemblage code: p = porcelaneous-dominated epiphytic assemblage (*Austrotrillina*+ soritids + peneroplids); r = rotalid-dominated epiphytic foraminiferal assemblage; v = victoriellid-dominated foraminiferal assemblage.

**Table 2:** Skeletal composition of the sand fraction within FA6 limestones as a function of depositional texture and foraminiferal assemblage.

| Sample | Dominant texture | Foraminiferal assemblage | Skeletal composition (%) | | | | | | | | | | | | | | | | |
|---|---|---|---|---|---|---|---|---|---|---|---|---|---|---|---|---|---|---|---|
| | | | *Austrotrillina* | Other miliolids | Soritids (*Sorites*, *Amphisorus*) | Peneroplids | Alveolinids | Agglutinated foram. | Victoriellids | *Neorotalia* | Other hyaline benthic foraminifers | Articulated coralline algae | Encrusting coralline algae | *Halimeda* | Mollusks | Echinoderm | Bryozoan | indeterminate |
| Well 96N002 : 4.00 m | P | p | 6 | 27 | | 8 | 1 | | 12 | | 4 | 7 | 19 | | 7 | 2 | | 7 |
| Well 96N002 : 6.00 m | G | p | 12 | 9 | 11 | | | 2 | | | 2 | 18 | 30 | | | 11 | 2 | 3 |
| Well 96N002 : 8.10 m | G | p | 4 | 17 | 21 | | | 7 | | 9 | 9 | 1 | 27 | | | 1 | | 4 |
| Well 96N002 : 11.10 m | P | v | | | | | | | 47 | 16 | 11 | 2 | 12 | | 2 | 7 | | 3 |
| Well 96N002 : 19.80 m | P | r | | 12 | 5 | | | | | 33 | 13 | 10 | 21 | | | | | 6 |
| Well 96N004 : 1.50 m | P | p | 1 | 15 | 12 | 5 | 1 | 5 | | 8 | 2 | 28 | 14 | | 2 | 3 | | 4 |
| Well 96N004 : 3.50 m | P | r | | 3 | 10 | | | 3 | 3 | 17 | 1 | 37 | 14 | | 1 | 4 | | 7 |
| Well 96N007 : 21.50 m | P | r | | 6 | | | | | 7 | 47 | 6 | 12 | 12 | | 3 | | | 7 |
| Well 99N008 : 24.70 m | P | r | | 2 | 2 | 1 | | 4 | | 41 | 9 | 9 | 14 | | 5 | 6 | | 7 |
| Well 99N008 : 9.40 m | P | p | 1 | 4 | 22 | | | 1 | 7 | 2 | 1 | 11 | 43 | | 2 | 3 | | 3 |
| Well 99N008 : 15.00 m | P | p | | 3 | 13 | | | | | 10 | 3 | 4 | 14 | 14 | 9 | 26 | | 4 |
| Well 99N012 : 8.80 m | P | v | | | | | | 1 | 39 | 39 | | 6 | 8 | | 1 | 3 | | 3 |
| Well 99N014 : 18.50 m | P | r | | 12 | 8 | | | 5 | 1 | 21 | 4 | 14 | 17 | | 4 | 6 | | 8 |
| Well 99N014: 27.80 m | P | p | | 2 | 19 | | | 2 | | 15 | 6 | 15 | 13 | 8 | 2 | 7 | 2 | 9 |
| Well 99N015: 16,25 m | FP | r | | 5 | | | | 2 | 2 | 43 | 5 | 10 | 22 | | 2 | 2 | | 7 |
| Well 99N017 : 11.75 m | P | p | 6 | 5 | 21 | | | 7 | 2 | | 6 | 21 | 15 | | 2 | 6 | | 9 |
| Well 99N017 : 22.00 m | P | p | | 3 | 22 | | | 4 | 2 | 14 | 6 | 16 | 14 | | 5 | 7 | | 7 |
| Well 99N017 : 22.05 m | P | p | 4 | 6 | 18 | | | 7 | 4 | 9 | 6 | 12 | 18 | | 2 | 6 | | 8 |
| Well GR07 : 11.10 m | G | p | | | 25 | | | 2 | 4 | 3 | 1 | 29 | 25 | | 2 | 4 | | 5 |
| CS26 (outcrop) | G | r | 4 | 5 | 1 | | | 10 | 6 | 21 | 4 | 23 | 9 | | 0 | 9 | | 8 |
| CS40 (outcrop) | FP | v | | 5 | 13 | | 2 | 4 | 20 | 8 | 4 | 14 | 16 | | 2 | 5 | | 7 |
| 045_01 (outcrop) | G | p | | 9 | 22 | | | 2 | | 4 | 8 | 7 | 33 | | **2** | 6 | | 7 |

**Table 1**: Skeletal composition of the sand-sized fraction (in %) of FA6 limestones (seagrass-related facies association) from point counting on thin-sections. The location of wells and outcrop samples is reported on Figure 4. Texture code: P=Packstone; G=Grainstone; FP: floatstone with packstone matrix. Foraminiferal assemblage code: p = porcelaneous-dominated epiphytic assemblage (*Austrotrillina*+ soritids + peneroplids); r = rotalid-dominated epiphytic foraminiferal assemblage; v = victoriellid-dominated foraminiferal assemblage.

| | | Skeletal composition (%) of the sand-sized fraction | | | | | | | | | |
|---|---|---|---|---|---|---|---|---|---|---|---|
| | | Epiphytic foraminifers* | Victoriellids | other benthic foraminifers | articulated RA | encrusting RA | Halimeda | Mollusk | Echinoderm | Bryozoan | indeterminate |
| All samples N=22 | Average | 30 | 7 | 15 | 14 | 19 | 1 | 3 | 6 | 0 | 6 |
| | min | 14 | 0 | 1 | 1 | 9 | 0 | 0 | 0 | 0 | 3 |
| | max | 47 | 47 | 33 | 37 | 43 | 14 | 9 | 26 | 2 | 9 |
| Grainstones N=5 | Average | 27 | 2 | 17 | 16 | 25 | 0 | 1 | 6 | 0 | 5 |
| | min | 23 | 0 | 3 | 1 | 9 | 0 | 0 | 1 | 0 | 3 |
| | max | 34 | 6 | 33 | 29 | 33 | 0 | 2 | 11 | 2 | 8 |
| Packstones N=17 | Average | 30 | 8 | 14 | 13 | 17 | 1 | 3 | 5 | 0 | 6 |
| | min | 14 | 0 | 1 | 2 | 12 | 0 | 0 | 0 | 0 | 3 |
| | max | 47 | 47 | 32 | 37 | 43 | 14 | 9 | 26 | 2 | 9 |
| Samples with porcelaneous-dominated epiphytic foraminiferal assemblage (N=12) | Average | 27 | 3 | 16 | 14 | 22 | 2 | 3 | 7 | 0 | 6 |
| | min | 14 | 0 | 3 | 1 | 13 | 0 | 0 | 1 | 0 | 3 |
| | max | 36 | 12 | 33 | 29 | 43 | 14 | 9 | 26 | 2 | 9 |
| Samples with calcarinid-dominated epiphytic foraminiferal assemblage (N=7) | Average | 36 | 3 | 16 | 16 | 16 | 0 | 2 | 4 | 0 | 7 |
| | min | 26 | 0 | 7 | 9 | 9 | 0 | 0 | 0 | 0 | 6 |
| | max | 47 | 7 | 25 | 37 | 22 | 0 | 5 | 9 | 0 | 8 |
| Samples with victoriellid-dominated foraminiferal assemblage (N=3) | Average | 24 | 34 | 9 | 7 | 14 | 0 | 2 | 5 | 0 | 4 |
| | min | 16 | 20 | 1 | 2 | 12 | 0 | 1 | 3 | 0 | 3 |
| | max | 36 | 47 | 15 | 14 | 16 | 0 | 2 | 7 | 0 | 7 |

**Table 2:** Skeletal composition of the sand fraction within FA6 limestones as a function of depositional texture and foraminiferal assemblage.

Figure 1

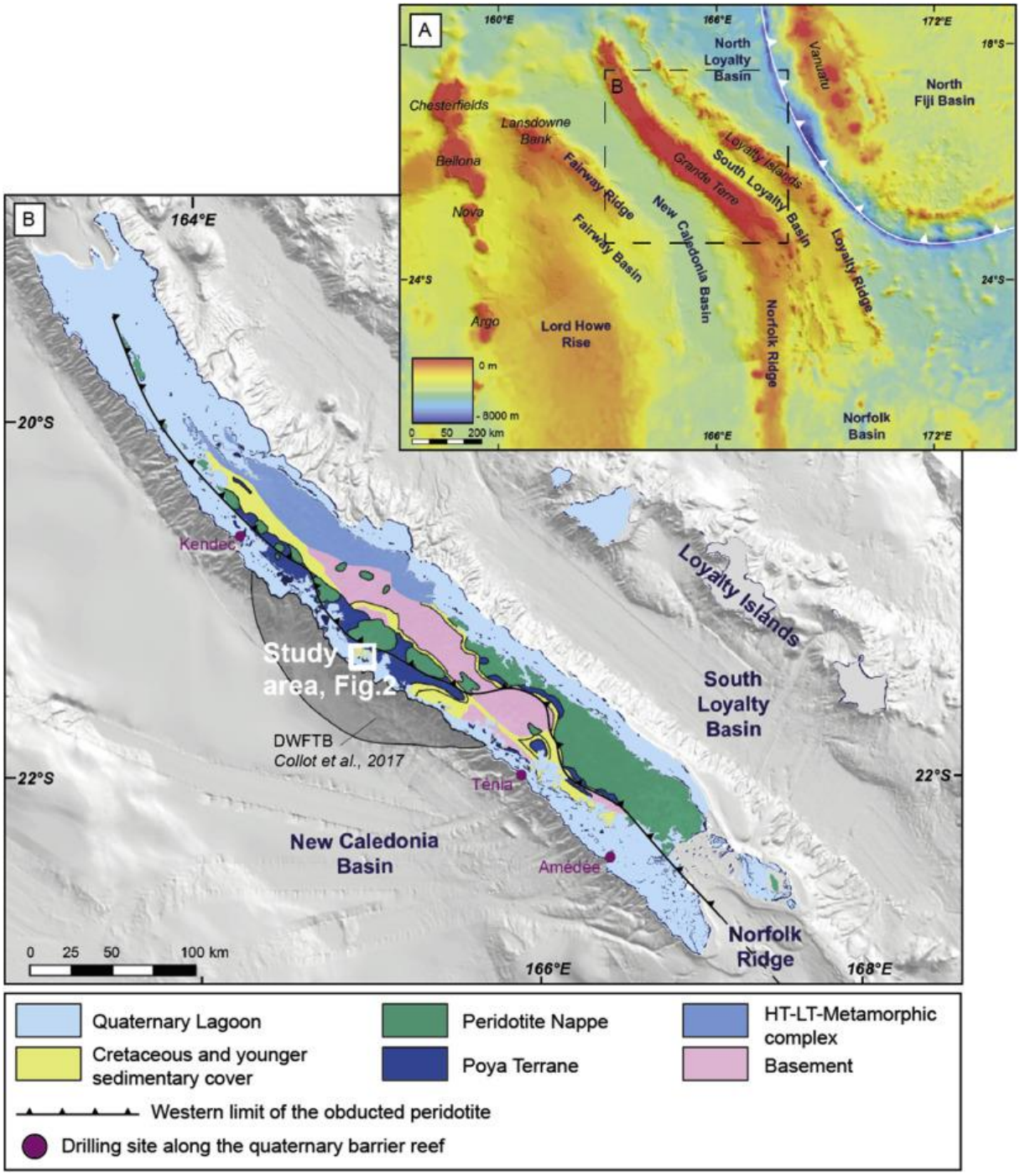
A
B
160°E
166°E
172°E
18°S
24°S
North Loyalty Basin
Vanuatu
North Fiji Basin
Chesterfields
Lansdowne Bank
Bellona
Fairway Ridge
Grande Terre
Loyalty Islands
South Loyalty Basin
Loyalty Ridge
Nova
New Caledonia Basin
Fairway Basin
Norfolk Ridge
Argo
Lord Howe Rise
0 m
- 8000 m
0 50 200 km
Norfolk Basin
B
164°E
20°S
22°S
Kendec
Study area, Fig.2
DWFTB
Collot et al., 2017
Tenia
Amedee
Loyalty Islands
South Loyalty Basin
New Caledonia Basin
Norfolk Ridge
0 25 50 100 km
166°E
168°E
Quaternary Lagoon
Cretaceous and younger sedimentary cover
Peridotite Nappe
Poya Terrane
HT-LT-Metamorphic complex
Basement
Western limit of the obducted peridotite
Drilling site along the quaternary barrier reef

Figure 2

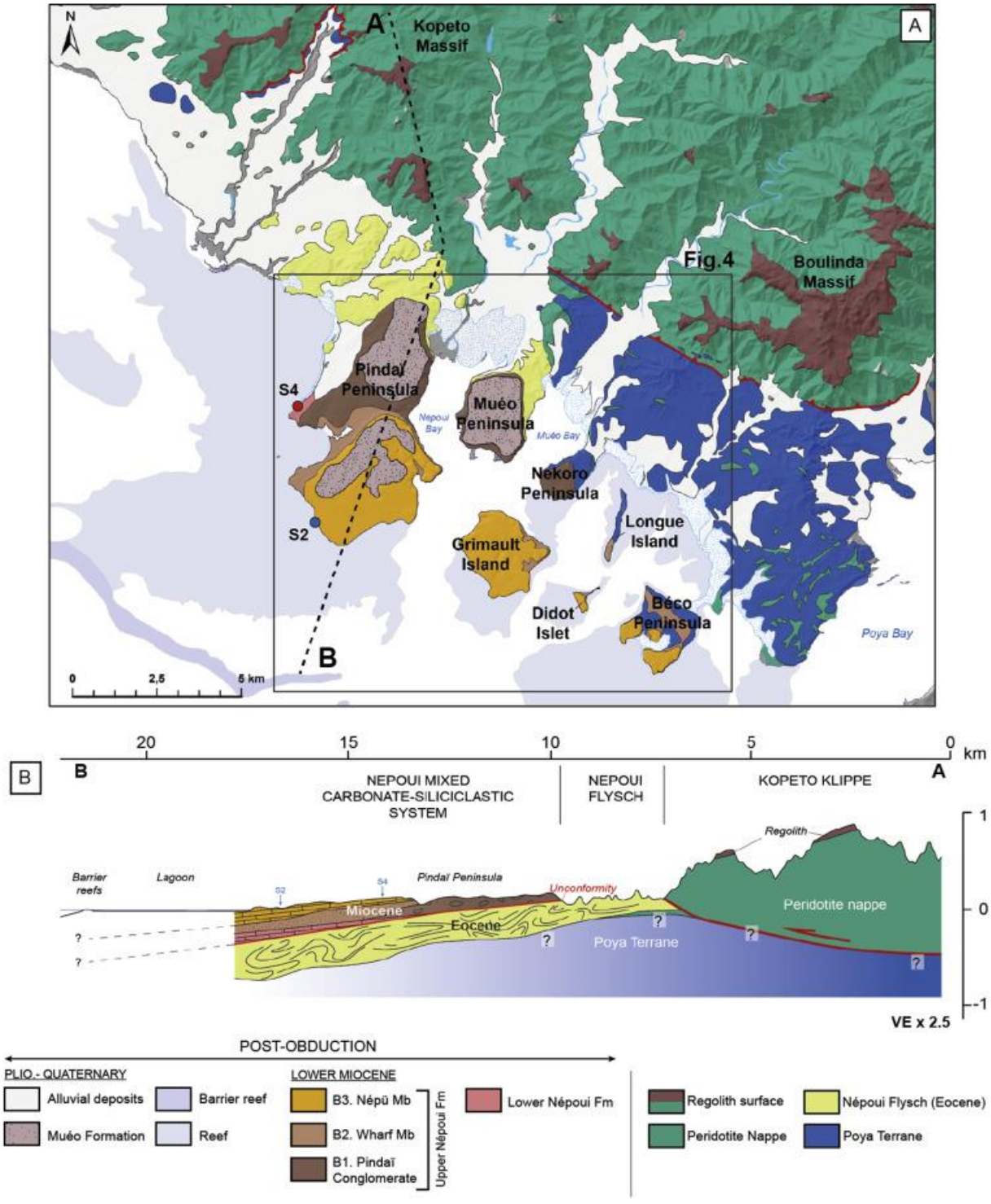
N
A
Kopeto Massif
A
Fig.4
Boulinda Massif
Pindaï Peninsula
S4
Muéo Peninsula
Nepoui Bay
Muéo Bay
Nékoro Peninsula
S2
Longue Island
Grimault Island
Didot Islet
Béco Peninsula
Poya Bay
B
0
2,5
5 km
20
15
10
5
0
km
B
B
NEPOUI MIXED CARBONATE-SILICICLASTIC SYSTEM
NEPOUI FLYSCH
KOPETO KLIPPE
A
Regolith
Barrier reefs
Lagoon
S2
S4
Pindaï Peninsula
Unconformity
Miocene
Eocene
Peridotite nappe
Poya Terrane
1
0
-1
VE x 2.5
POST-OBDUCTION
PLIO.- QUATERNARY
Alluvial deposits
Barrier reef
Muéo Formation
Reef
LOWER MIOCENE
B3. Népü Mb
B2. Wharf Mb
B1. Pindaï Conglomerate
Upper Népoui Fm
Lower Népoui Fm
Regolith surface
Népoui Flysch (Eocene)
Peridotite Nappe
Poya Terrane

Figure 3

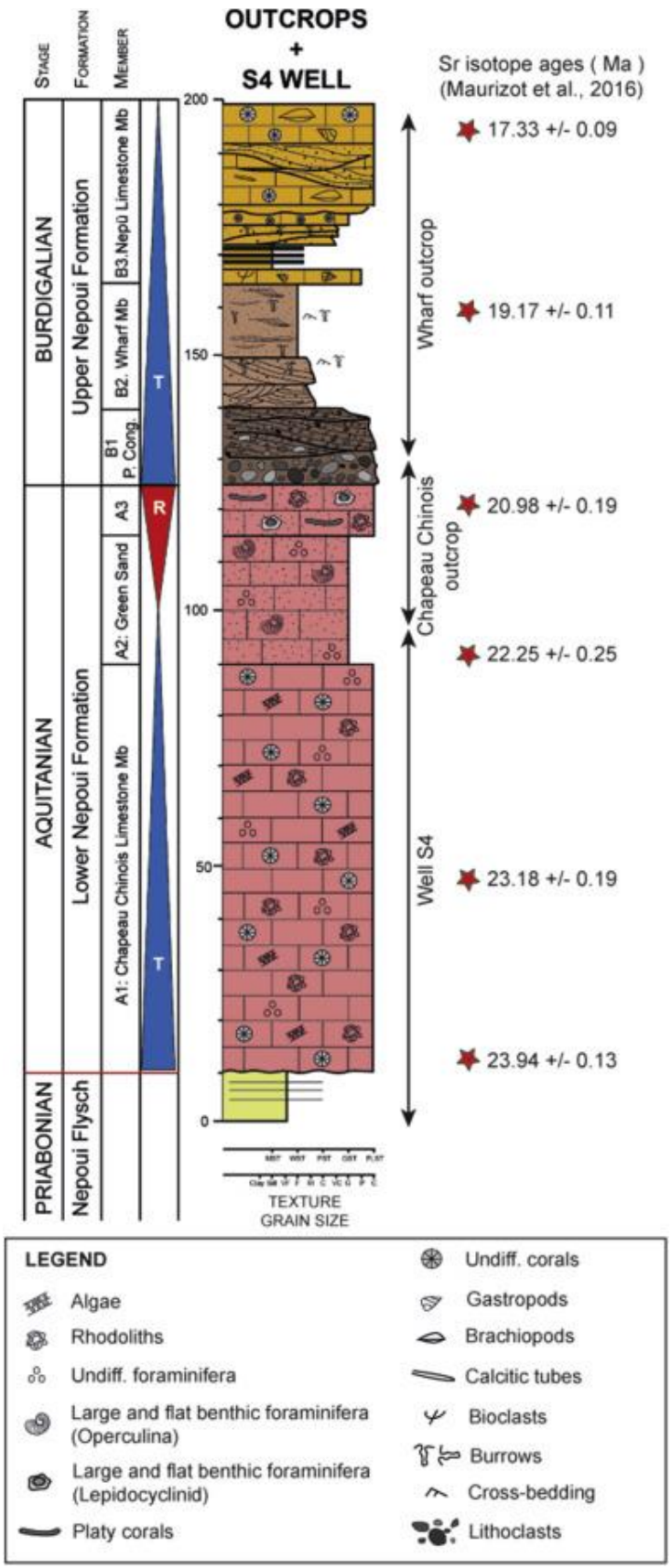
STAGE
FORMATION
MEMBER
OUTCROPS
+
S4 WELL
Sr isotope ages ( Ma )
(Maurizot et al., 2016)
BURDIGALIAN
AQUITANIAN
PRIABONIAN
Upper Nepoui Formation
Lower Nepoui Formation
Nepoui Flysch
B3.Nepü Limestone Mb
B2. Wharf Mb
B1 P. Cong.
A3
A2: Green Sand
A1: Chapeau Chinois Limestone Mb
T
R
T
200
150
100
50
0
17.33 +/- 0.09
19.17 +/- 0.11
20.98 +/- 0.19
22.25 +/- 0.25
23.18 +/- 0.19
23.94 +/- 0.13
Wharf outcrop
Chapeau Chinois outcrop
Well S4
TEXTURE
GRAIN SIZE
LEGEND
Algae
Rhodoliths
Undiff. foraminifera
Large and flat benthic foraminifera (Operculina)
Large and flat benthic foraminifera (Lepidocyclinid)
Platy corals
Undiff. corals
Gastropods
Brachiopods
Calcitic tubes
Bioclasts
Burrows
Cross-bedding
Lithoclasts

Figure 4

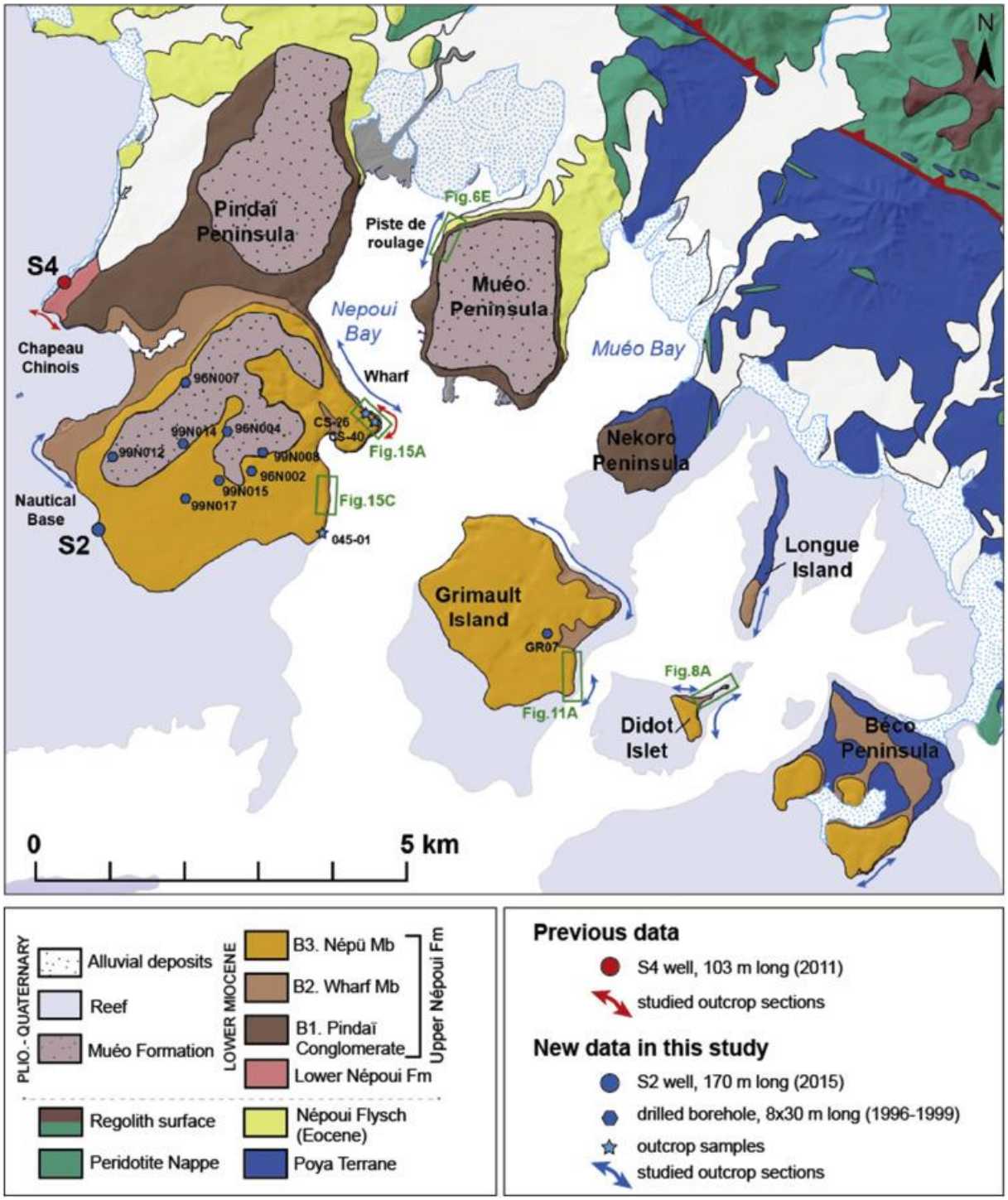
N
Pindaï Peninsula
S4
Chapeau Chinois
Piste de roulage
Fig.6E
Muéo Peninsula
Nepoui Bay
Muéo Bay
Wharf
96N007
99N014
96N004
99N012
99N008
96N002
99N015
99N017
CS-26
CS-40
Fig.15A
Fig.15C
Nautical Base
S2
045-01
Nekoro Peninsula
Longue Island
Grimault Island
GR07
Fig.8A
Fig.11A
Didot Islet
Béco Peninsula
0
5 km
PLIO.-QUATERNARY
Alluvial deposits
Reef
Muéo Formation
LOWER MIOCENE
B3. Népü Mb
B2. Wharf Mb
B1. Pindaï Conglomerate
Upper Népoui Fm
Lower Népoui Fm
Regolith surface
Népoui Flysch (Eocene)
Peridotite Nappe
Poya Terrane
Previous data
S4 well, 103 m long (2011)
studied outcrop sections
New data in this study
S2 well, 170 m long (2015)
drilled borehole, 8x30 m long (1996-1999)
outcrop samples
studied outcrop sections

Figure 5

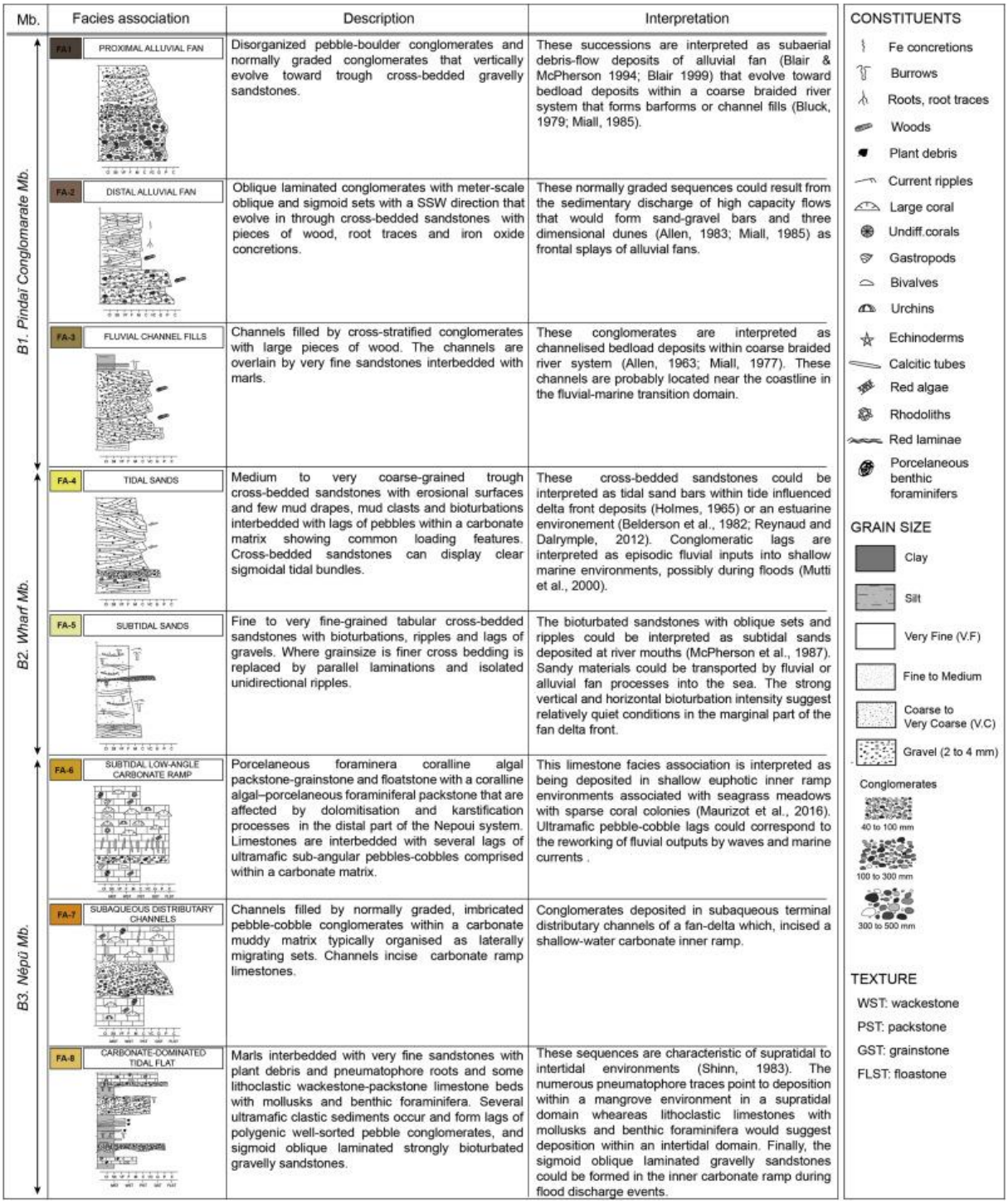
Mb.
Facies association
Description
Interpretation
B1. Pindaï Conglomarate Mb.
B2. Wharf Mb.
B3. Népui Mb.
FA-1
PROXIMAL ALLUVIAL FAN
Disorganized pebble-boulder conglomerates and normally graded conglomerates that vertically evolve toward trough cross-bedded gravelly sandstones.
These successions are interpreted as subaerial debris-flow deposits of alluvial fan (Blair & McPherson 1994; Blair 1999) that evolve toward bedload deposits within a coarse braided river system that forms barforms or channel fills (Bluck, 1979; Miall, 1985).
FA-2
DISTAL ALLUVIAL FAN
Oblique laminated conglomerates with meter-scale oblique and sigmoid sets with a SSW direction that evolve in through cross-bedded sandstones with pieces of wood, root traces and iron oxide concretions.
These normally graded sequences could result from the sedimentary discharge of high capacity flows that would form sand-gravel bars and three dimensional dunes (Allen, 1983; Miall, 1985) as frontal splays of alluvial fans.
FA-3
FLUVIAL CHANNEL FILLS
Channels filled by cross-stratified conglomerates with large pieces of wood. The channels are overlain by very fine sandstones interbedded with marls.
These conglomerates are interpreted as channelised bedload deposits within coarse braided river system (Allen, 1963; Miall, 1977). These channels are probably located near the coastline in the fluvial-marine transition domain.
FA-4
TIDAL SANDS
Medium to very coarse-grained trough cross-bedded sandstones with erosional surfaces and few mud drapes, mud clasts and bioturbations interbedded with lags of pebbles within a carbonate matrix showing common loading features. Cross-bedded sandstones can display clear sigmoidal tidal bundles.
These cross-bedded sandstones could be interpreted as tidal sand bars within tide influenced delta front deposits (Holmes, 1965) or an estuarine environement (Belderson et al., 1982; Reynaud and Dalrymple, 2012). Conglomeratic lags are interpreted as episodic fluvial inputs into shallow marine environments, possibly during floods (Mutti et al., 2000).
FA-5
SUBTIDAL SANDS
Fine to very fine-grained tabular cross-bedded sandstones with bioturbations, ripples and lags of gravels. Where grainsize is finer cross bedding is replaced by parallel laminations and isolated unidirectional ripples.
The bioturbated sandstones with oblique sets and ripples could be interpreted as subtidal sands deposited at river mouths (McPherson et al., 1987). Sandy materials could be transported by fluvial or alluvial fan processes into the sea. The strong vertical and horizontal bioturbation intensity suggest relatively quiet conditions in the marginal part of the fan delta front.
FA-6
SUBTIDAL LOW-ANGLE CARBONATE RAMP
Porcelaneous foraminera coralline algal packstone-grainstone and floatstone with a coralline algal–porcelaneous foraminiferal packstone that are affected by dolomitisation and karstification processes in the distal part of the Nepoui system. Limestones are interbedded with several lags of ultramafic sub-angular pebbles-cobbles comprised within a carbonate matrix.
This limestone facies association is interpreted as being deposited in shallow euphotic inner ramp environments associated with seagrass meadows with sparse coral colonies (Maurizot et al., 2016). Ultramafic pebble-cobble lags could correspond to the reworking of fluvial outputs by waves and marine currents .
FA-7
SUBAQUEOUS DISTRIBUTARY CHANNELS
Channels filled by normally graded, imbricated pebble-cobble conglomerates within a carbonate muddy matrix typically organised as laterally migrating sets. Channels incise carbonate ramp limestones.
Conglomerates deposited in subaqueous terminal distributary channels of a fan-delta which, incised a shallow-water carbonate inner ramp.
FA-8
CARBONATE-DOMINATED TIDAL FLAT
Marls interbedded with very fine sandstones with plant debris and pneumatophore roots and some lithoclastic wackestone-packstone limestone beds with mollusks and benthic foraminifera. Several ultramafic clastic sediments occur and form lags of polygenic well-sorted pebble conglomerates, and sigmoid oblique laminated strongly bioturbated gravelly sandstones.
These sequences are characteristic of supratidal to intertidal environments (Shinn, 1983). The numerous pneumatophore traces point to deposition within a mangrove environment in a supratidal domain wheareas lithoclastic limestones with mollusks and benthic foraminifera would suggest deposition within an intertidal domain. Finally, the sigmoid oblique laminated gravelly sandstones could be formed in the inner carbonate ramp during flood discharge events.
CONSTITUENTS
Fe concretions
Burrows
Roots, root traces
Woods
Plant debris
Current ripples
Large coral
Undiff.corals
Gastropods
Bivalves
Urchins
Echinoderms
Calcitic tubes
Red algae
Rhodoliths
Red laminae
Porcelaneous benthic foraminifers
GRAIN SIZE
Clay
Silt
Very Fine (V.F)
Fine to Medium
Coarse to Very Coarse (V.C)
Gravel (2 to 4 mm)
Conglomerates
40 to 100 mm
100 to 300 mm
300 to 500 mm
TEXTURE
WST: wackestone
PST: packstone
GST: grainstone
FLST: floastone

Figure 6

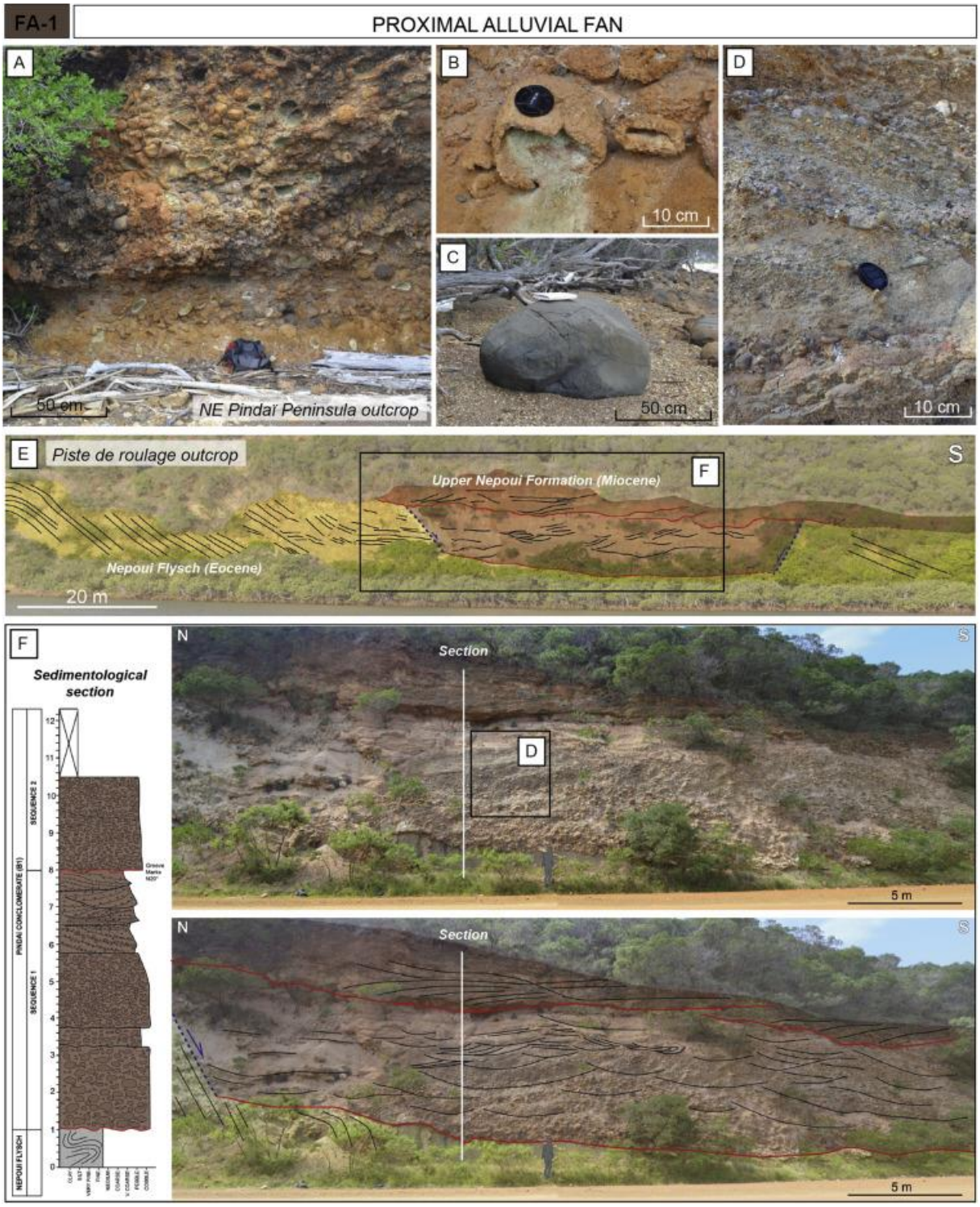
FA-1
PROXIMAL ALLUVIAL FAN
A
50 cm
NE Pindaï Peninsula outcrop
B
10 cm
C
50 cm
D
10 cm
E
Piste de roulage outcrop
S
Upper Nepoui Formation (Miocene)
F
Nepoui Flysch (Eocene)
20 m
F
Sedimentological section
N
Section
D
S
5 m
N
Section
S
5 m

Figure 7

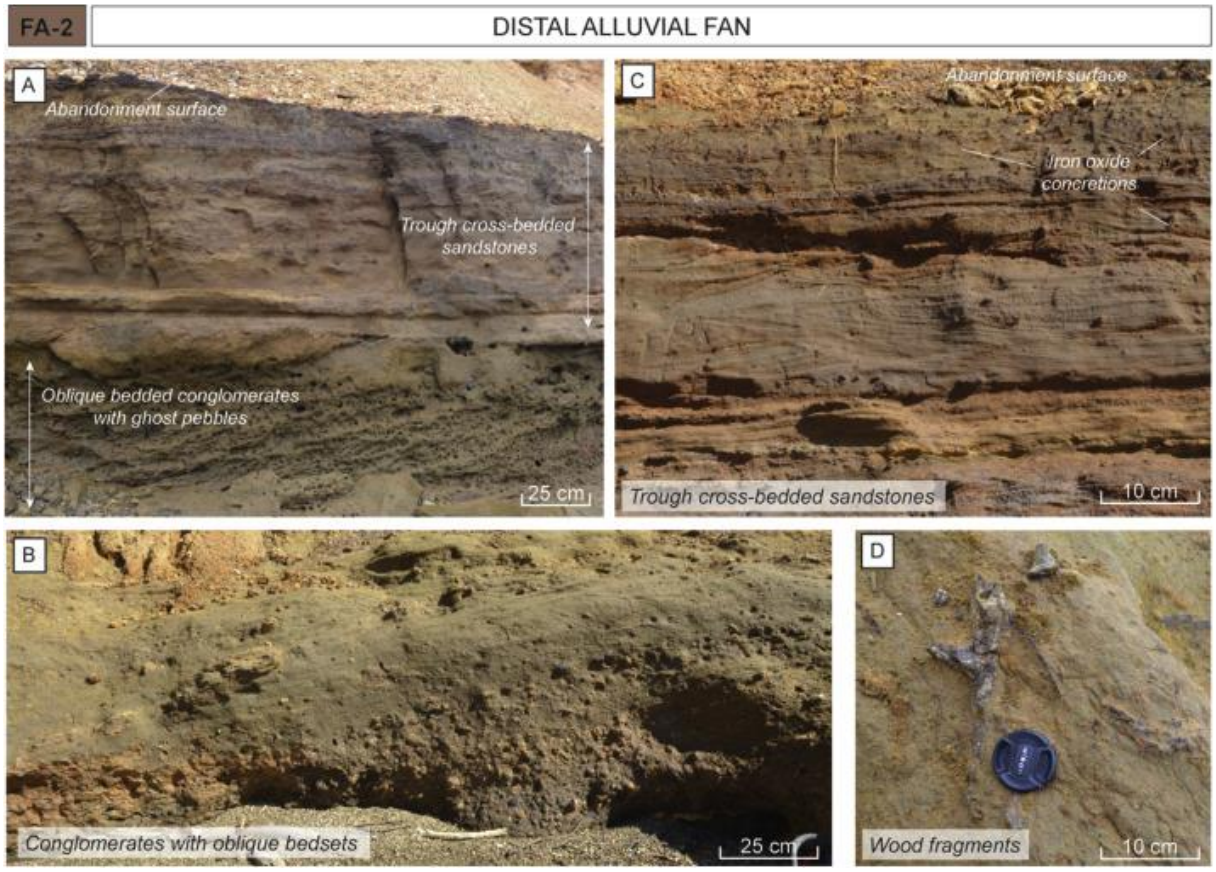
FA-2
DISTAL ALLUVIAL FAN
A
Abandonment surface
Trough cross-bedded sandstones
Oblique bedded conglomerates with ghost pebbles
25 cm
C
Abandonment surface
Iron oxide concretions
Trough cross-bedded sandstones
10 cm
B
Conglomerates with oblique bedsets
25 cm
D
Wood fragments
10 cm

Figure 8

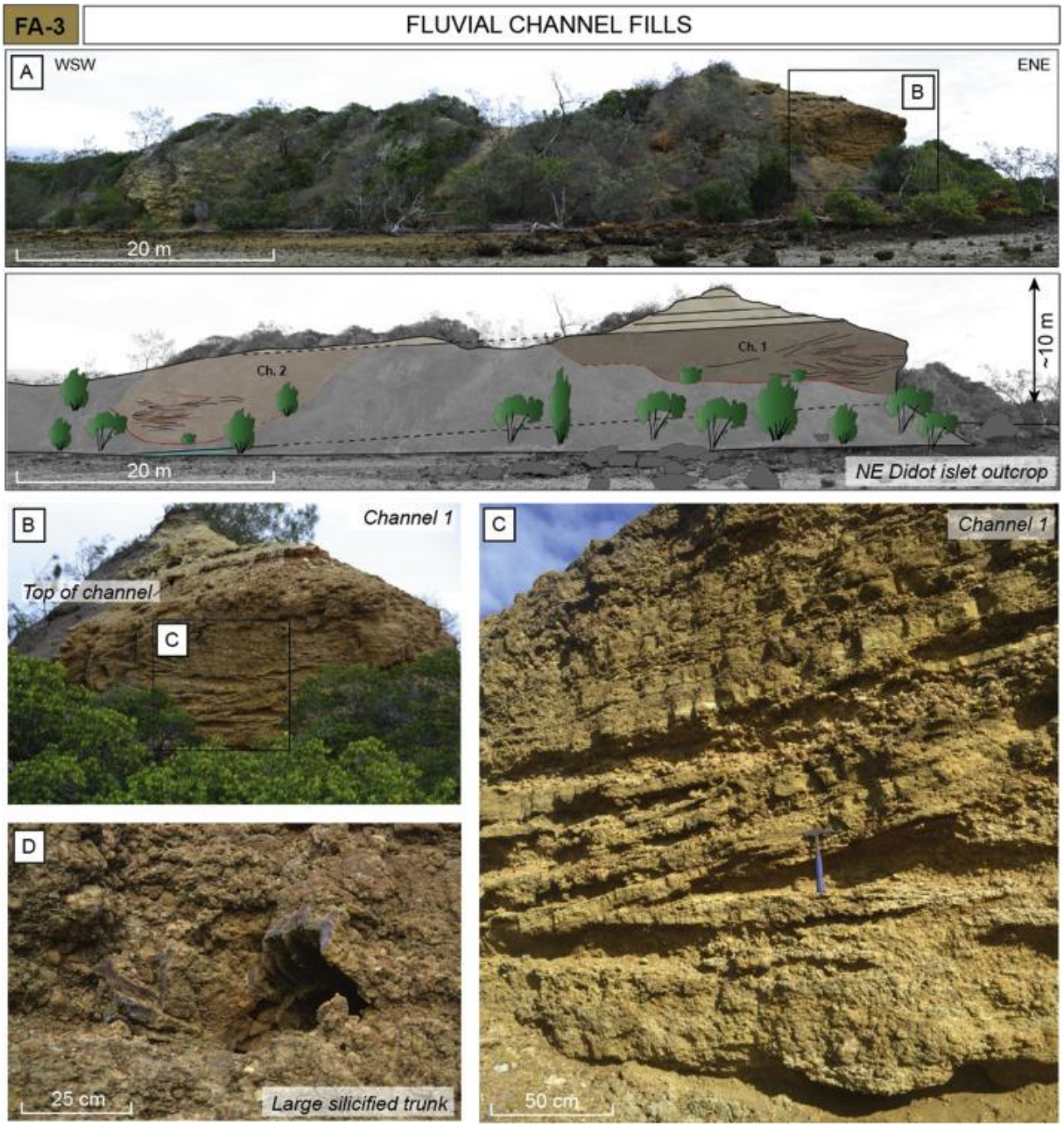
FA-3
FLUVIAL CHANNEL FILLS
A
WSW
ENE
B
20 m
Ch. 1
Ch. 2
~10 m
20 m
NE Didot islet outcrop
B
Channel 1
Top of channel
C
C
Channel 1
D
25 cm
Large silicified trunk
50 cm

Figure 9

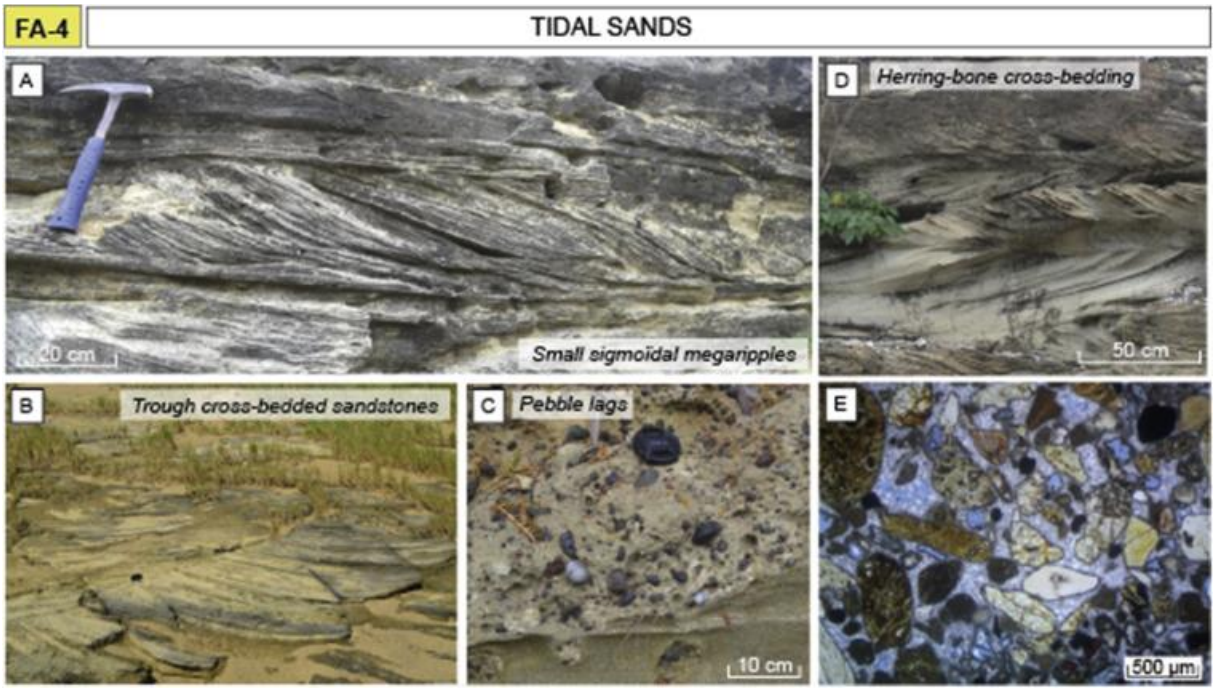


Figure 10

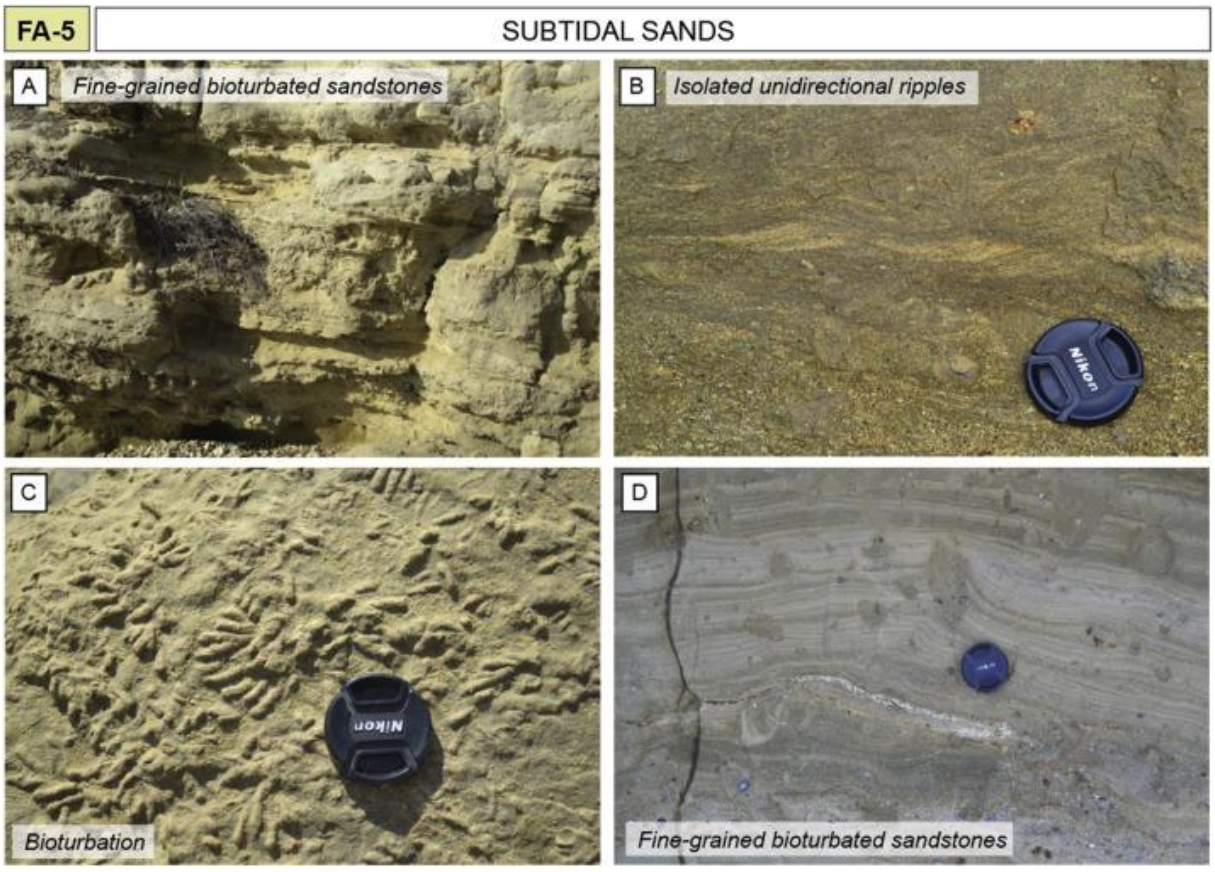

Figure 11

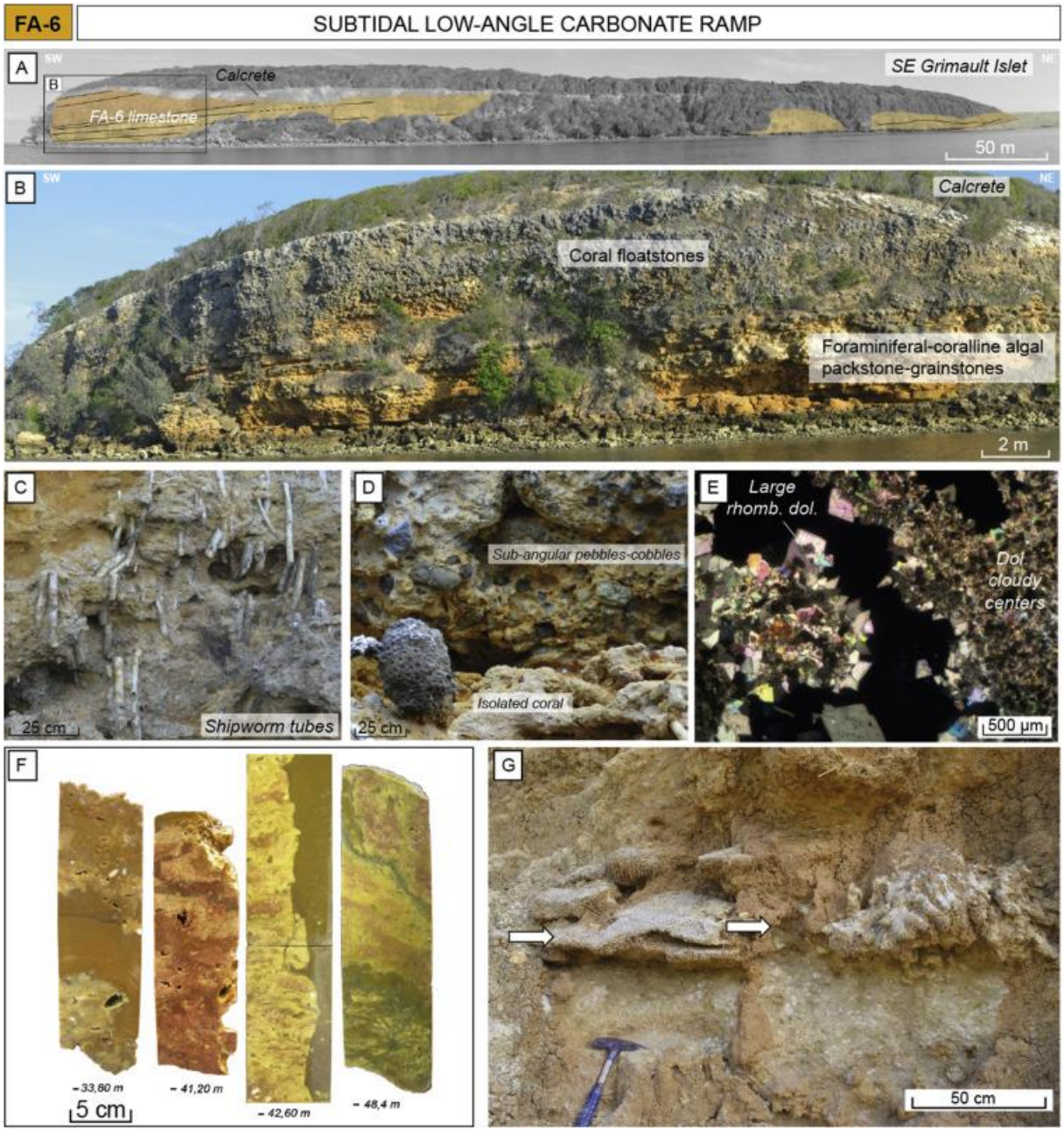
FA-6
SUBTIDAL LOW-ANGLE CARBONATE RAMP
A
SW
B
Calcrete
FA-6 limestone
SE Grimault Islet
NE
50 m
B
SW
Calcrete
NE
Coral floatstones
Foraminiferal-coralline algal packstone-grainstones
2 m
C
25 cm
Shipworm tubes
D
Sub-angular pebbles-cobbles
Isolated coral
25 cm
E
Large rhomb. dol.
Dol. cloudy centers
500 µm
F
- 33,60 m
- 41,20 m
- 42,60 m
- 48,4 m
5 cm
G
50 cm

Figure 12

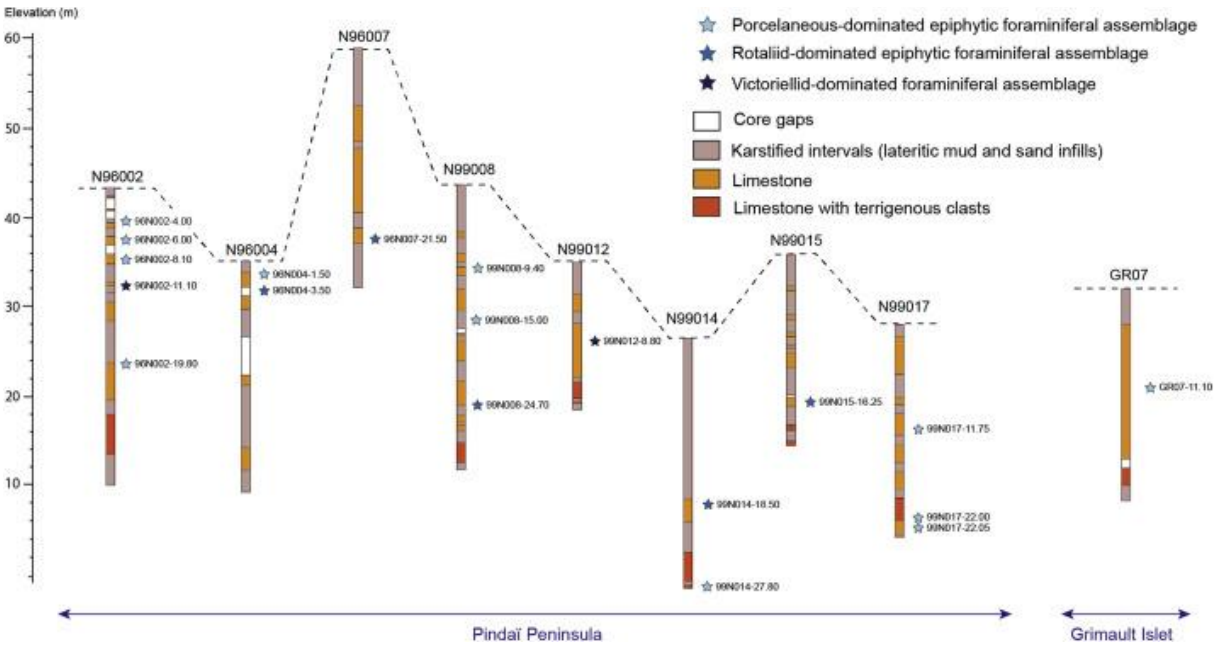
Elevation (m)
60
50
40
30
20
10
Porcelaneous-dominated epiphytic foraminiferal assemblage
Rotaliid-dominated epiphytic foraminiferal assemblage
Victoriellid-dominated foraminiferal assemblage
Core gaps
Karstified intervals (lateritic mud and sand infills)
Limestone
Limestone with terrigenous clasts
N96002
N96004
N96007
N99008
N99012
N99014
N99015
N99017
GR07
Pindaï Peninsula
Grimault Islet

Figure 13

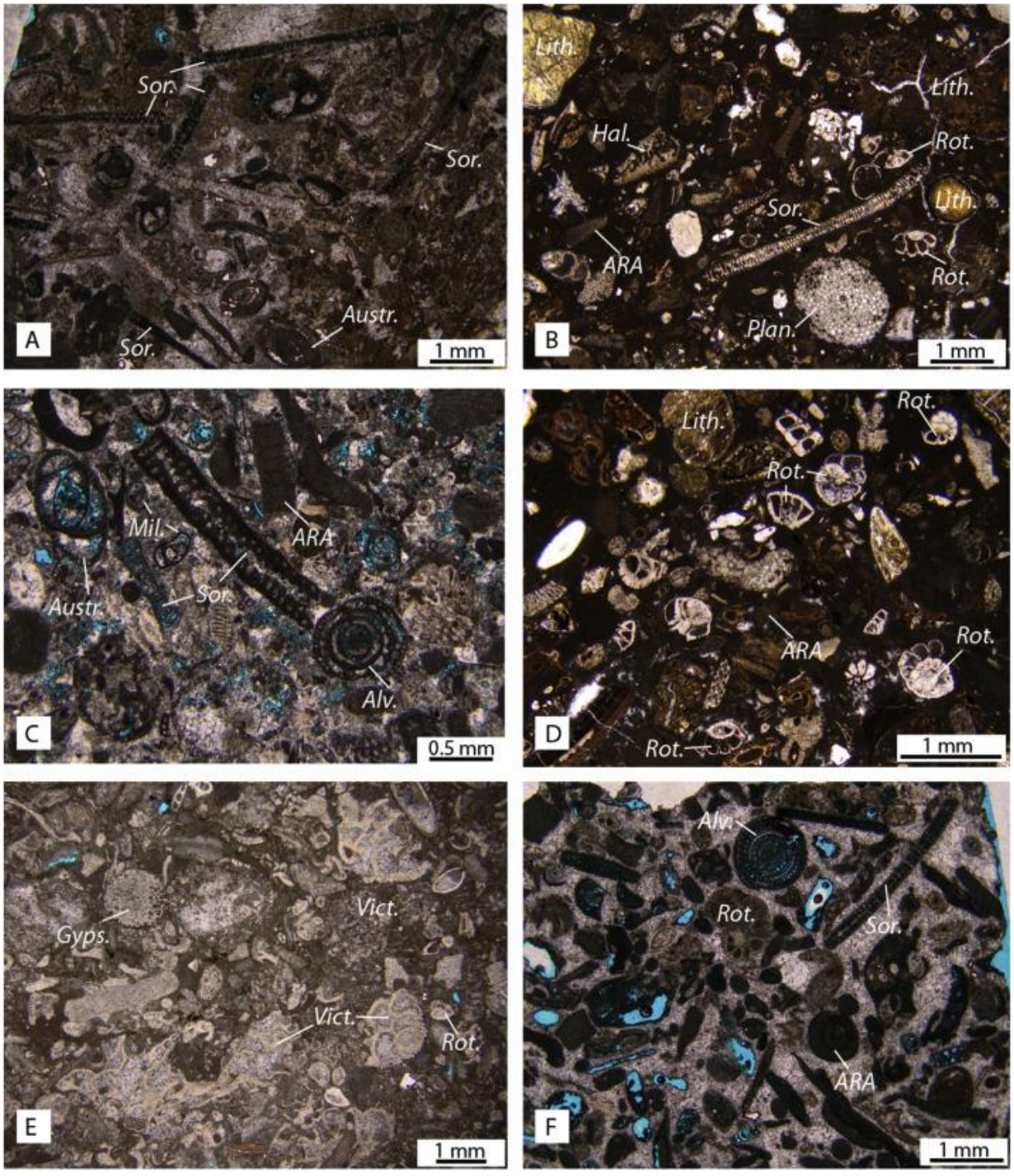
Sor.
Sor.
Austr.
Sor.
A
1 mm
Lith.
Lith.
Hal.
Rot.
Sor.
Lith.
ARA
Rot.
Plan.
B
1 mm
Mil.
ARA
Austr.
Sor.
Alv.
C
0.5 mm
Lith.
Rot.
Rot.
ARA
Rot.
Rot.
D
1 mm
Gyps.
Vict.
Vict.
Rot.
E
1 mm
Alv.
Rot.
Sor.
ARA
F
1 mm

Figure 14

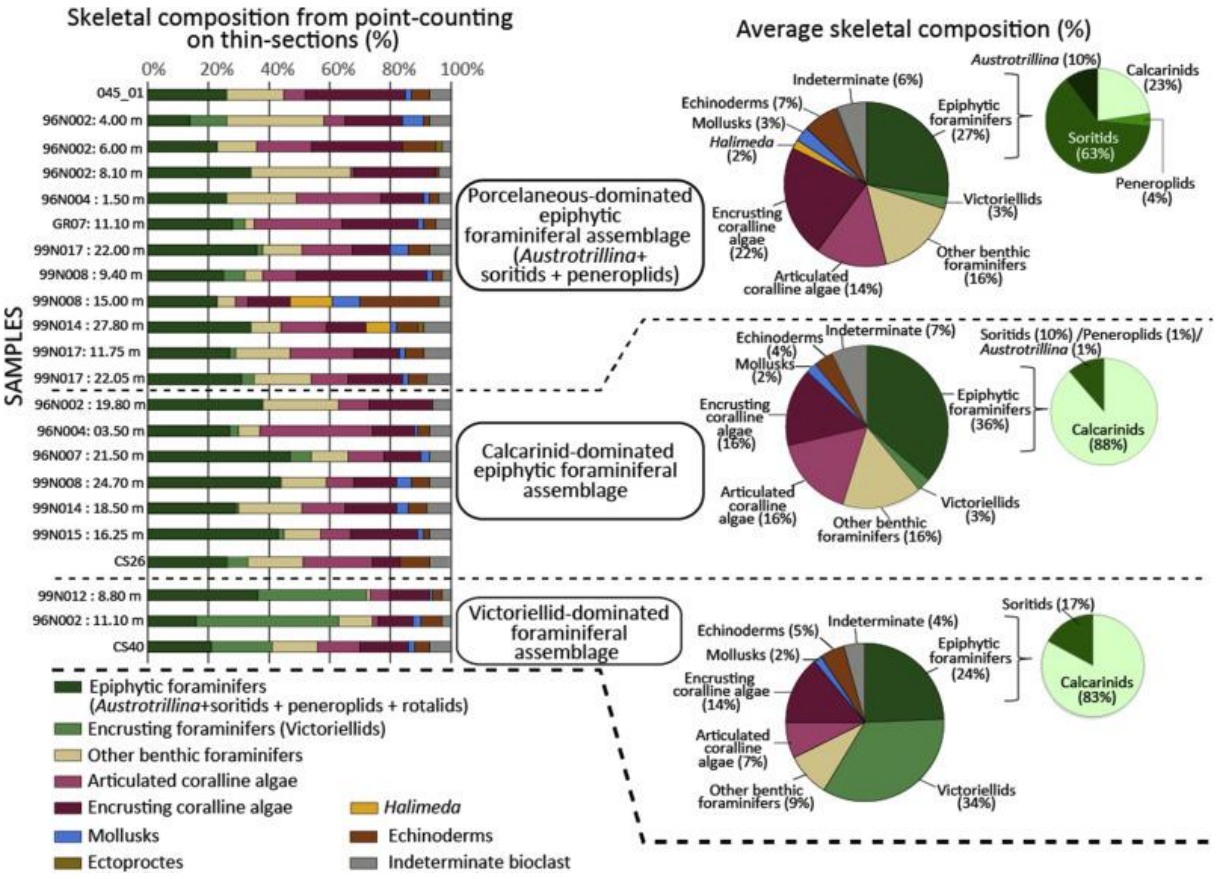
Skeletal composition from point-counting on thin-sections (%)
0%
20%
40%
60%
80%
100%
SAMPLES
045_01
96N002: 4.00 m
96N002: 6.00 m
96N002: 8.10 m
96N004 : 1.50 m
GR07: 11.10 m
99N017 : 22.00 m
99N008 : 9.40 m
99N008 : 15.00 m
99N014 : 27.80 m
99N017: 11.75 m
99N017 : 22.05 m
96N002 : 19.80 m
96N004: 03.50 m
96N007 : 21.50 m
99N008 : 24.70 m
99N014 : 18.50 m
99N015 : 16.25 m
CS26
99N012 : 8.80 m
96N002 : 11.10 m
CS40
Porcelaneous-dominated epiphytic foraminiferal assemblage (Austrotrillina+ soritids + peneroplids)
Calcarinid-dominated epiphytic foraminiferal assemblage
Victoriellid-dominated foraminiferal assemblage
Epiphytic foraminifers (Austrotrillina+soritids + peneroplids + rotalids)
Encrusting foraminifers (Victoriellids)
Other benthic foraminifers
Articulated coralline algae
Encrusting coralline algae
Mollusks
Ectoproctes
Halimeda
Echinoderms
Indeterminate bioclast
Average skeletal composition (%)
Indeterminate (6%)
Echinoderms (7%)
Mollusks (3%)
Halimeda (2%)
Encrusting coralline algae (22%)
Articulated coralline algae (14%)
Other benthic foraminifers (16%)
Victoriellids (3%)
Epiphytic foraminifers (27%)
Austrotrillina (10%)
Calcarinids (23%)
Soritids (63%)
Peneroplids (4%)
Indeterminate (7%)
Echinoderms (4%)
Mollusks (2%)
Encrusting coralline algae (16%)
Articulated coralline algae (16%)
Other benthic foraminifers (16%)
Victoriellids (3%)
Epiphytic foraminifers (36%)
Soritids (10%) /Peneroplids (1%)/ Austrotrillina (1%)
Calcarinids (88%)
Indeterminate (4%)
Echinoderms (5%)
Mollusks (2%)
Encrusting coralline algae (14%)
Articulated coralline algae (7%)
Other benthic foraminifers (9%)
Victoriellids (34%)
Epiphytic foraminifers (24%)
Soritids (17%)
Calcarinids (83%)

Figure 15

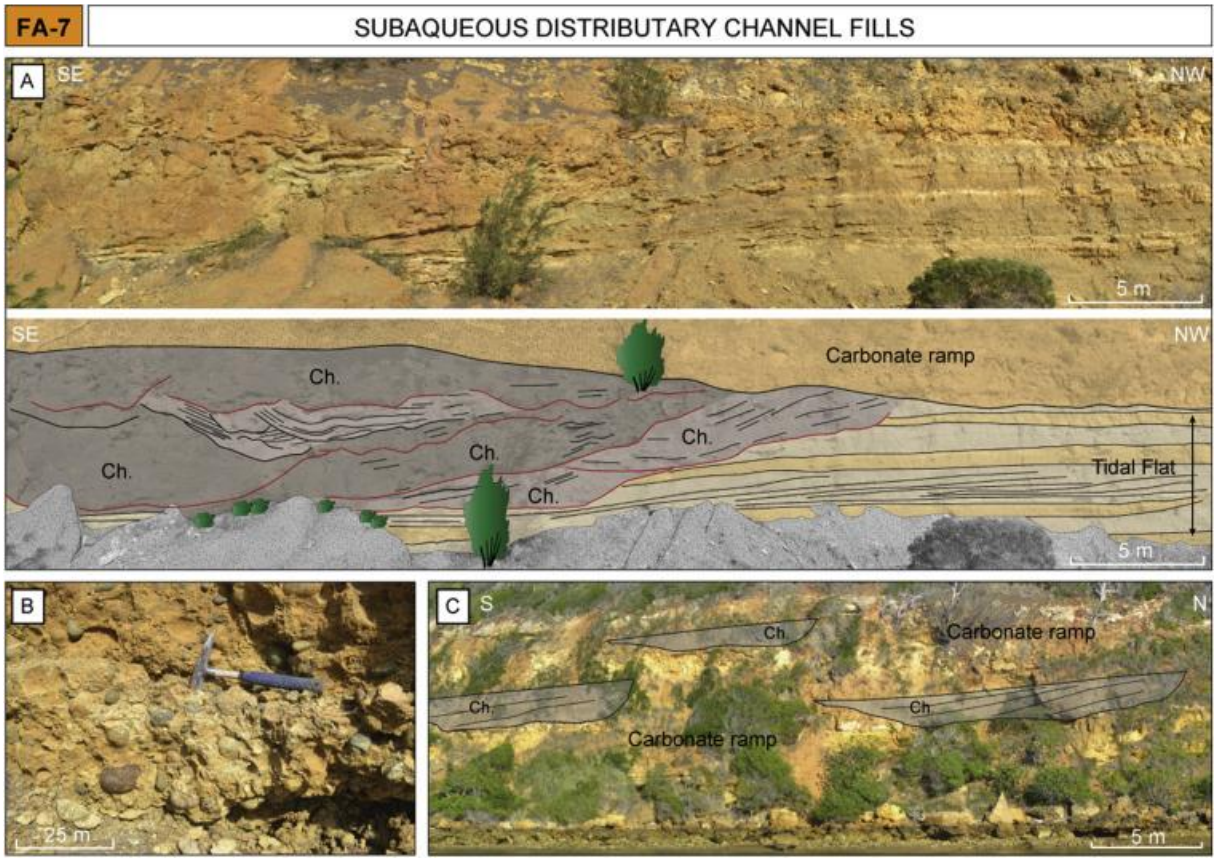
FA-7
SUBAQUEOUS DISTRIBUTARY CHANNEL FILLS
A
SE
NW
5 m
SE
NW
Carbonate ramp
Ch.
Ch.
Ch.
Ch.
Ch.
Tidal Flat
5 m
B
25 m
C
S
N
Ch.
Carbonate ramp
Ch.
Ch.
Carbonate ramp
5 m

Figure 16

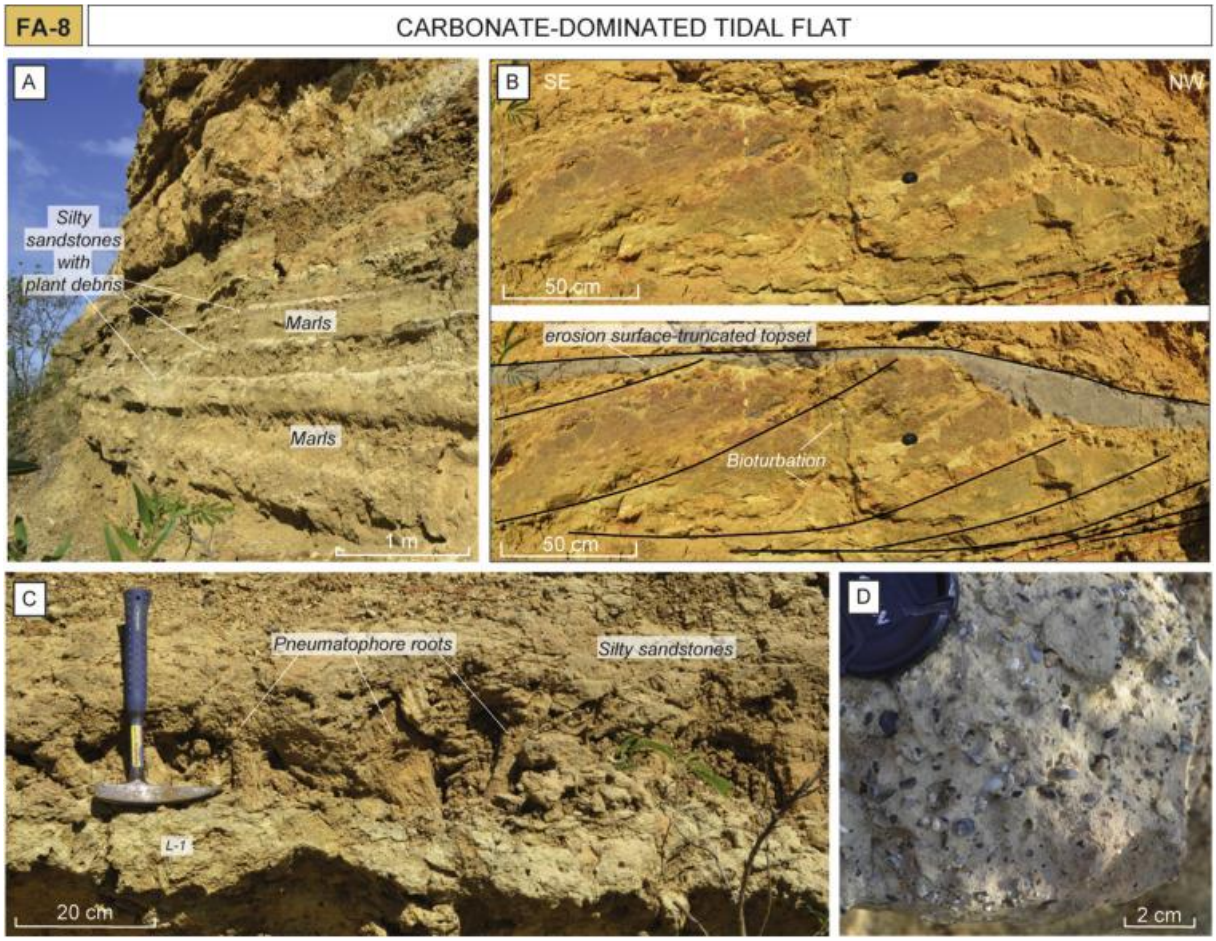
FA-8
CARBONATE-DOMINATED TIDAL FLAT
A
Silty sandstones with plant debris
Marls
Marls
1 m
B
SE
NW
50 cm
erosion surface-truncated topset
Bioturbation
50 cm
C
Pneumatophore roots
Silty sandstones
L-1
20 cm
D
2 cm

Figure 17

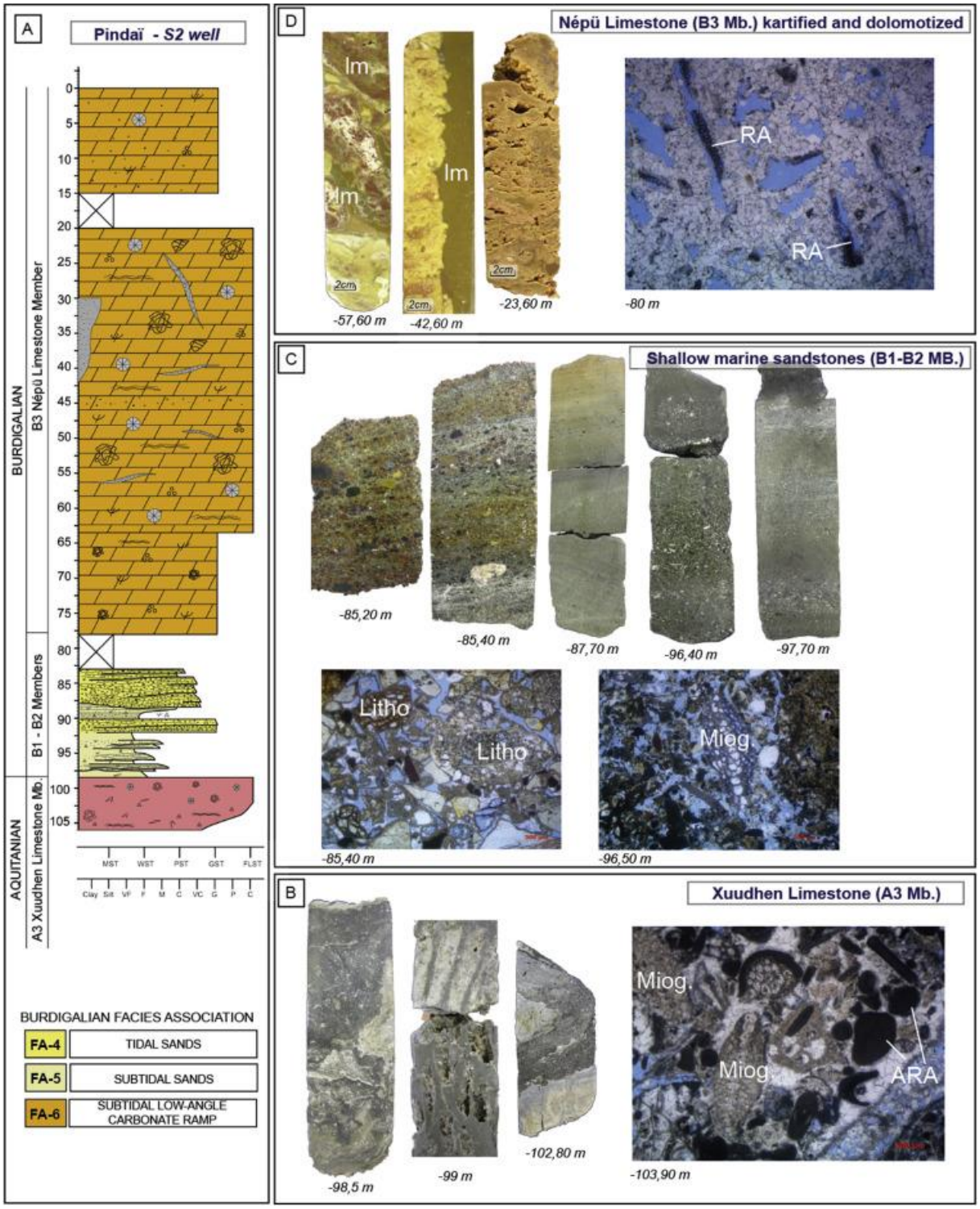
A
Pindaï - S2 well
BURDIGALIAN
B3 Népü Limestone Member
B1 - B2 Members
AQUITANIAN
A3 Xuudhen Limestone Mb.
MST
WST
PST
GST
FLST
Clay Silt VF F M C VC G P C
BURDIGALIAN FACIES ASSOCIATION
FA-4 TIDAL SANDS
FA-5 SUBTIDAL SANDS
FA-6 SUBTIDAL LOW-ANGLE CARBONATE RAMP
D
Népü Limestone (B3 Mb.) kartified and dolomotized
lm
2cm
-57,60 m
-42,60 m
-23,60 m
RA
-80 m
C
Shallow marine sandstones (B1-B2 MB.)
-85,20 m
-85,40 m
-87,70 m
-96,40 m
-97,70 m
Litho
-85,40 m
Mieg
-96,50 m
B
Xuudhen Limestone (A3 Mb.)
-98,5 m
-99 m
-102,80 m
Miog.
ARA
-103,90 m

Figure 18

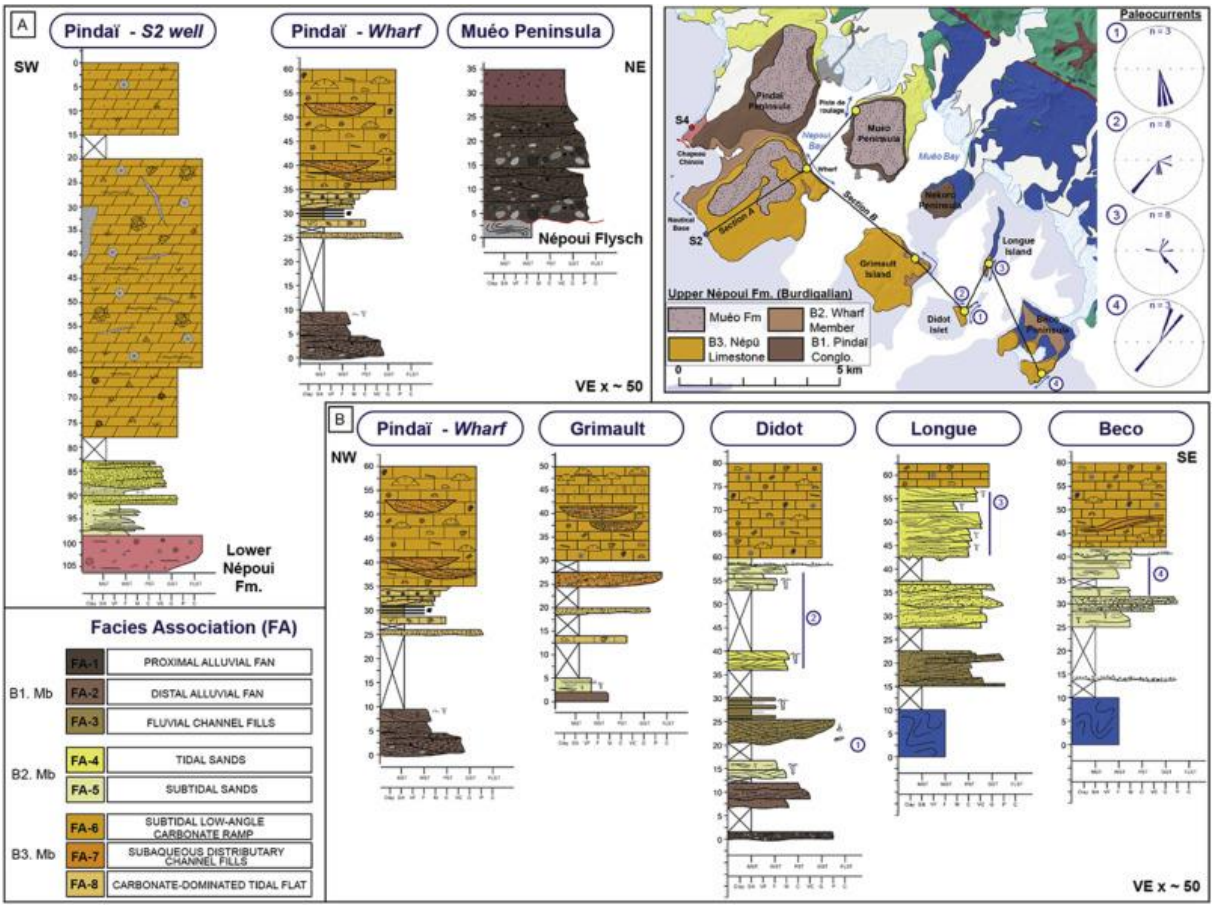
A
Pindaï - S2 well
Pindaï - Wharf
Muéo Peninsula
SW
NE
Népoui Flysch
VE x ~ 50
Lower Népoui Fm.
Paleocurrents
Upper Népoui Fm. (Burdigalian)
Muéo Fm
B2. Wharf Member
B3. Népû Limestone
B1. Pindaï Conglo.
0
5 km
Facies Association (FA)
B1. Mb
B2. Mb
B3. Mb
FA-1 PROXIMAL ALLUVIAL FAN
FA-2 DISTAL ALLUVIAL FAN
FA-3 FLUVIAL CHANNEL FILLS
FA-4 TIDAL SANDS
FA-5 SUBTIDAL SANDS
FA-6 SUBTIDAL LOW-ANGLE CARBONATE RAMP
FA-7 SUBAQUEOUS DISTRIBUTARY CHANNEL FILLS
FA-8 CARBONATE-DOMINATED TIDAL FLAT
B
Pindaï - Wharf
Grimault
Didot
Longue
Beco
NW
SE
VE x ~ 50

Figure 19

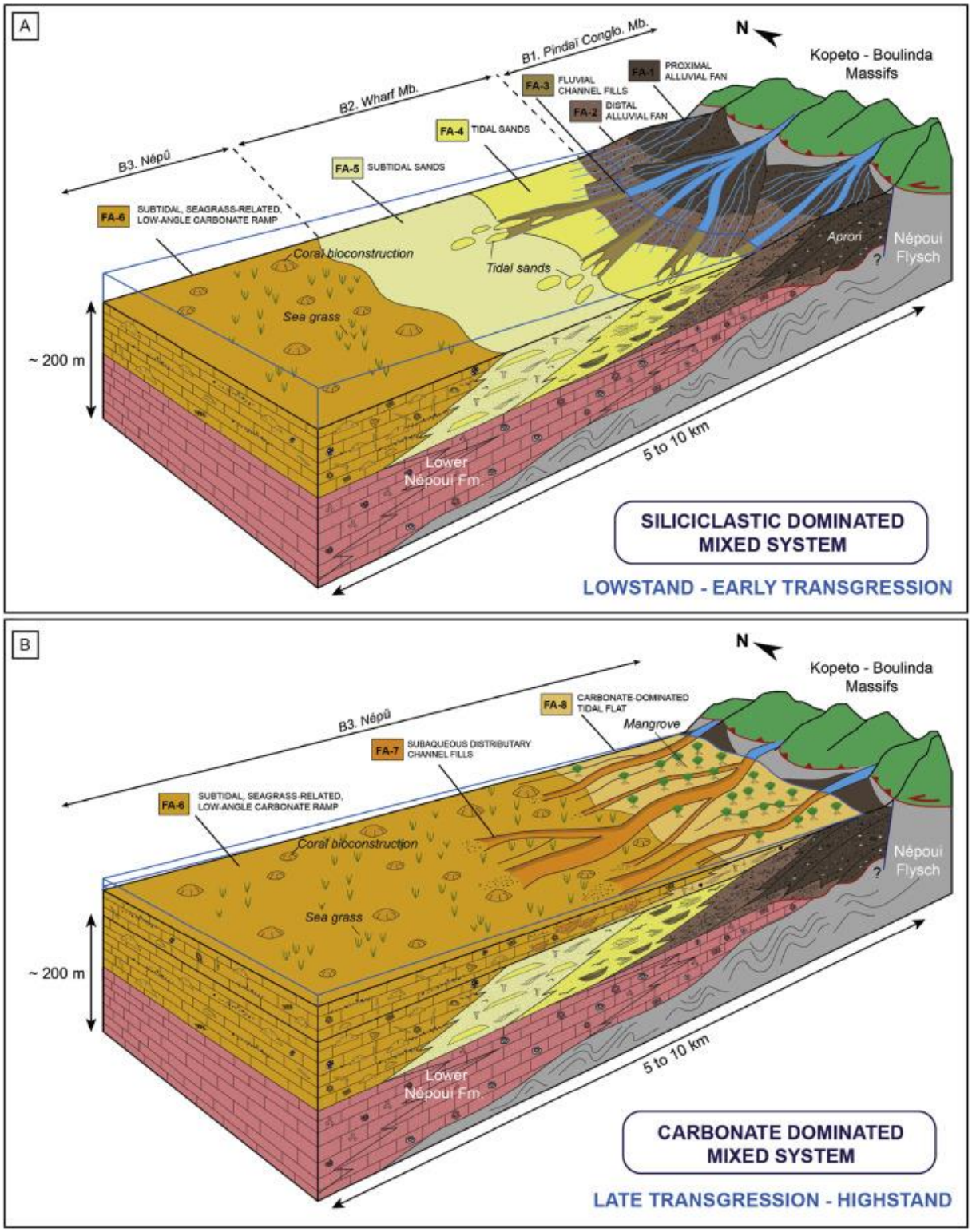
A
N
B1. Pindaï Conglo. Mb.
B2. Wharf Mb.
B3. Népû
FA-1 PROXIMAL ALLUVIAL FAN
FA-3 FLUVIAL CHANNEL FILLS
FA-2 DISTAL ALLUVIAL FAN
FA-4 TIDAL SANDS
FA-5 SUBTIDAL SANDS
FA-6 SUBTIDAL, SEAGRASS-RELATED, LOW-ANGLE CARBONATE RAMP
Kopeto - Boulinda Massifs
Aprori
Népoui Flysch
Coral bioconstruction
Tidal sands
Sea grass
~ 200 m
Lower Népoui Fm.
5 to 10 km
SILICICLASTIC DOMINATED MIXED SYSTEM
LOWSTAND - EARLY TRANSGRESSION
B
N
B3. Népû
FA-8 CARBONATE-DOMINATED TIDAL FLAT
Mangrove
FA-7 SUBAQUEOUS DISTRIBUTARY CHANNEL FILLS
FA-6 SUBTIDAL, SEAGRASS-RELATED, LOW-ANGLE CARBONATE RAMP
Kopeto - Boulinda Massifs
Coral bioconstruction
Sea grass
Népoui Flysch
~ 200 m
Lower Népoui Fm.
5 to 10 km
CARBONATE DOMINATED MIXED SYSTEM
LATE TRANSGRESSION - HIGHSTAND